NASA CONTRACTOR REPORT

NASA CR-1066

NARROW BAND CROSS-CORRELATION ANALYSIS OF FLUCTUATING PRESSURES BENEATH A TURBULENT BOUNDARY LAYER

by C. M. Ailman and A. S. Hopkins

Prepared by
DOUGLAS AIRCRAFT COMPANY
Santa Monica, Calif.
for Langley Research Center

NATIONAL AERONAUTICS AND SPACE ADMINISTRATION • WASHINGTON, D. C. • MAY 1968

NASA CR-1066

NARROW BAND CROSS-CORRELATION ANALYSIS OF FLUCTUATING PRESSURES BENEATH A TURBULENT BOUNDARY LAYER

By C. M. Ailman and A. S. Hopkins

Issued by Originator as Report No. DAC-60874

Prepared under Contract No. NAS 1-6901 by
DOUGLAS AIRCRAFT COMPANY
Santa Monica, Calif.

for Langley Research Center

NATIONAL AERONAUTICS AND SPACE ADMINISTRATION

For sale by the Clearinghouse for Federal Scientific and Technical Information
Springfield, Virginia 22151 – CFSTI price $3.00

ACKNOWLEDGEMENT

The authors wish to acknowledge the contributions made to this study by D. E. Hines, Douglas Missile and Space Systems Division, Structures Department. The investigation was supported by the National Aeronautics and Space Administration under contract number NAS1-6901 and was technically monitored by Mr. Harvey Hubbard, Dynamics Load Division, Langley Research Center.

CONTENTS

FIGURES

TABLES

NARROW BAND CROSS-CORRELATION ANALYSIS OF FLUCTUATING PRESSURES BENEATH A TURBULENT BOUNDARY LAYER

By C. M. Ailman and A. S. Hopkins

SUMMARY

Selected narrow-band cross-correlations were calculated for pressure fluctuations at a rigid wall under both a uniform and a disturbed turbulent boundary layer at supersonic speeds. Flow disturbances resulted from: (1) a forward-facing step-spoiler, (2) an aft-facing step (with a well-behaved, slowly growing turbulent boundary layer prior to the step); and (3) an impinging (and reflected) shock generated by an obstruction to the airstream some distance from the wall. The data are presented in terms of contours of equal correlation coefficient ($\tau = 0$), spatial decays of the correlation, and convection velocities. Included in the discussions are:

(1) Separability of the temporal and spatial variables

(2) Mathematical descriptors of the frequency-dependent cross-correlations

(3) Convection velocity

(4) Frequency dependency variations with locations in the flow

(5) Laterally convected pressure signature behind an aft-facing step

(6) Comparison of the data with different theories

1. INTRODUCTION

Fluctuating pressures at a rigid surface were measured beneath two-dimensional, turbulent, supersonic boundary layers which could be described as well-behaved, and disturbed by forward-facing steps, aft-facing steps, and shock waves. In a previous report (ref. 1), the data were presented as spectra and broad band correlation information. Such information is necessary to define environments for flight vehicles, but not sufficient if modal analysis for local exterior structure is to be performed.

The purpose of the narrow band study documented in this report is to provide detailed information on those characteristics which indicated a dependence on frequency. To achieve this goal, selected narrow band cross-correlation analysis of the fluctuating pressures was performed for each kind of flow condition available. These narrow band cross-correlations were then used, in complement with the inherent frequency information available within broadband cross-correlation calculations, to describe the frequency dependencies. The results are presented for the three narrow bands of frequencies examined, and extensive discussions are included on their interpretation. Mathematical descriptors and comparisons with theory are also included. In all instances, the results have been generalized to boundary layer parameters which were fully reported in ref. 1 and are tabulated again in this document.

2. SYMBOLS

A	Normalized autocorrelation
A', R', C', R'_x, R'_z	Unnormalized correlations
B	Resolution bandwidth (radians/sec)
C	Normalized correlation coefficient ($\tau = 0$)
c	Speed of sound (ft/sec)
c_f	Coefficient of friction at the wall
dB, ΔdB	Decibels or difference in decibels respectively (re 0.0002 dynes/cm^2)
FPL's	Fluctuating pressure levels in dB
H	Form factor (nondimensional) = δ^*/θ
Hz	Hertz (= cps)
h	Step height (in.)
k	Wave number (in.$^{-1}$)
K	Rate of change of phase with frequency (deg/H_2)
L	Length of panel in direction of flow (in.)
N	Noise level (lb/in.^{2})^2
P_α	Amplitude of the PSD at some frequency (lb/in.^{2})^2/Hz
$P_{\alpha\beta}$	Amplitude of the cross-PSD at some frequency (lbs/in.^{2})^2/Hz
PSD	Power spectral density
q	Free-stream dynamic pressure (lbs/in.^{2})
Q	Dynamic amplification factor

R	Normalized cross-correlation
R_e	Reynolds number (in.$^{-1}$)
R_x	Normalized cross-correlation in the direction of the flow ($\xi_z = 0$)
R_z	Normalized cross-correlation in the direction perpendicular to the flow ($\xi_x = 0$)
RM	Normalized cross-correlation in frame of reference moving with the boundary layer
RM_a	Separable factor of RM
RT	Normalized cross-correlation in retarded time frame of reference
RT_a	Separable factor of RT
S	Signal level (lb/in.^{2})^2
T	Length of record (sec)
U_c	Convection velocity (in. /sec)
U_2	Free-stream velocity behind a shock wave (in. /sec)
U_∞	Free-stream velocity (in. /sec)
U_L	Resultant velocity (in. /sec)
W	Width of panel in direction perpendicular to the flow (in.)
α	Longitudinal decay rate
β	Lateral decay rate
γ^2_{xy}	Coherence function
δ	Boundary layer thickness (in.)
δ^*	Boundary layer displacement thickness (in.)
Δ	Filter bandwidth (radians/sec)
ϵ	Error factor
η_x	Spatial separation in retarded-time frame of reference (in.)

η_τ	Temporal displacement in retarded-time frame of reference (sec)
θ	Boundary layer momentum thickness (in.)
Λ_{xy}	Equivalent area of perfect correlation ($in.^2$)
ν_∞	Free-stream viscosity ($lb\text{-}sec/in.^2$)
ξ_x	Spatial separation in the direction of the flow (in.)
ξ_z	Spatial separation perpendicular to the flow (in.)
τ	Time displacement (sec)
τ'	Basic incremental time displacement (sec)
τ_o	Time displacement at which maximum correlation occurs (sec)
τ_w	Wall shear stress ($lb/in.^2$)
ψ_x	Spatial separation in frame of reference moving with the boundary layer (in.)
ψ_τ	Temporal displacement in frame of reference moving with the boundary layer (sec)
ω	Frequency (radians/sec)
ω_c	Nyquist frequency or cutoff frequency (radians/sec)
ω_o	Center frequency (radians/sec)

3. SOURCE OF DATA

The data on which this study is based were obtained in tests described in detail in reference 1. Nevertheless, it seems appropriate to recapitulate some of the more pertinent facts. Paragraphs 3.1 through 3.3 are extractions of previously published subject matter and may be omitted by those readers familiar with the previous work. However, paragraphs 3.4 and 3.5 describe factors peculiar to this study alone.

3.1 Facility Description

The data were obtained by fluctuating pressure sensors mounted in rigid, two-dimensional, geometrical configurations on the sidewall of the trisonic, 1-ft, blowdown wind tunnel at the Douglas Aerophysics Laboratory. Only supersonic data are considered in this report. The basic wind tunnel description may be found in reference 2. Modifications to the facility were made to eliminate background noise associated with choked-valve operation. These modifications are described in reference 3.

Four basic types of flow were examined for the detailed characteristics of the fluctuating pressures: undisturbed, forward- and aft-facing steps, and shock-disturbed. In all cases, the flow-disturbing geometries spanned the tunnel wall from floor to ceiling, resulting in two-dimensional flow near the center of the tunnel wall. The forward-facing step was generated by a 3/4 in. high step-spoiler about 1.3 in. deep, while the aft-facing steps were a result of a long insert extending clear into the stilling chamber. A well-behaved turbulent boundary layer was developed on the insert before its abrupt ending some 3/4 in. above the sidewall plane. For the shock-disturbed flow, a 7.5° shock wave generator was utilized as described in reference 3. The shock produced by the generating body had a shock strength (ratio of plateau pressure behind the shock to free-stream static pressure) of 1.86 and impinged within the instrumented portion of the sidewall. That shock strength was sufficient to cause separation of the flow behind the position of impingement.

The static pressure distributions for each of the various flows were reported in reference 1. Boundary layer probes permitted definition of boundary layer parameters upstream of all disturbances. The resultant flow descriptors are given below in paragraph 3.2.

3.2 Flow Parameters

Based on data interpretations and calculations as outlined in reference 1, flow descriptions (table 1) were obtained for the condition of undisturbed flow prior to any disturbances.

3.3 Measurement Techniques

Two types of fluctuating pressure sensors were utilized during testing: condensor microphones (Brüel and Kjaer Model 4136) and piezoelectric transducers (Atlantic Research Corporation LD 107-M1). The frequency range of recorded data and the finite size of the sensing elements were such that pressure cancellation effects were in evidence at the high frequencies. However, for this study, the frequencies examined were low enough that such corrections could be neglected (less than 1 dB). System corrections, sensitivity corrections, static pressure corrections, etc. were likewise negligible, and hence not included. More complete details of the electronics and system corrections are contained in reference 1. It is sufficient to state here that data utilized in this study were not affected by these factors. The error discussion in paragraph 3.5 details other influencing factors affecting the results of this study.

The facility, being a blow-down tunnel, had a finite time during which the tunnel parameters stabilized. During this short test period (10 to 15 sec), a slight variation of stagnation pressure was in evidence, causing a continuous but slight time variation of all the parameters. The fall-off was minimized by tying into a large reservoir of air. This minor time variation can be shown to give results comparable to invariant conditions (stationarity) for the small time sample intervals during which data are examined. (See par. 4.4 for a discussion justifying the stationarity assumption for a much more strongly time-dependent function.)

3.4 Data Reduction

The intent of this study was to perform narrow band cross-correlation calculations on data previously recorded on magnetic tape. From such calculations, the statistical similarity of a pressure signature at one position in time and space to the signature at some different but nearby position may be found for various frequency ranges. The procedure for comparison was:

(1) The tapes were played back by means of a 14-track tape deck and playback amplifiers. The calibration data were played back to establish levels and frequency sensitivities for each track, and phase differences between tracks.

(2) The broad band voltage signal from step 1 was filtered to obtain narrow bands of data (using electrical analog-type filters manufactured by the Brüel and Kjaer Co.).

TABLE 1

UNDISTURBED BOUNDARY LAYER FLOW DESCRIPTORS

Mach No.	U_∞(fps)	q_∞(psi)	δ(in.)	δ^*(in.)	θ(in.)	H	$R_e(\text{in.}^{-1}) \times 10^6$	c_f	τ_w(psi)	ν_∞ $10^9\left(\frac{\text{lb-sec}}{\text{in.}^2}\right)$
1.41 (a)	1328	9.74	0.330	0.0655	0.0300	2.18	0.62	0.00189	0.0184	2.11
3.45	2110	12.08	0.812	0.3304	0.0493	6.70	1.08	0.00085	0.0102	0.88
3.48 (a)	2140	11.75	0.805	0.3240	0.0490	6.62	1.05	0.00085	0.00997	0.785

[a]Aft-facing step (0.38 in. upstream of step face).

(3) Segments of the filtered data from step 2 were digitized during periods of stationary data (where stationarity implies that mean and mean-squared values are not varying with time).

(4) The product of typical signals were time-averaged over a fixed record length of time T, with different time delays interjected between them.

The result of the first four steps was a cross-correlation in time of different locations in space, or in the usual notation, a space-time cross-correlation of a narrow band pressure signature. Mathematically, this is defined as

$$R'_{1,2}(\vec{\xi}, \tau, \omega) = \lim_{T \to \infty} \frac{1}{T} \int_{-T/2}^{T/2} p_1(\vec{x}, t, \omega)\, p_2(\vec{x} + \vec{\xi},\ t + \tau,\ \omega)\, dt \qquad (1)$$

where $R'_{1,2}(\vec{\xi}, \tau, \omega)$ is the space time cross-correlation of two pressures, p_1 and p_2, measured at spatial locations $\vec{x}$ and $\vec{x} + \vec{\xi}$ which have had their signature filtered in the frequency domain and are thus dependent on ω.

R' is assumed to be calculated with use of data which are stationary and ergodic, so R' is dependent only on the spatial separation vector $\vec{\xi}$ (between locations 1 and 2) and the time differences τ (introduced mechanically between the time histories of p_1 and p_2). It has been shown (ref. 4) that equation 1 can be replaced by a finite summation process. Since this is a more suitable format for the computer, the following type of summation was performed:

$$R'_{1,2}(\vec{\xi}, \tau, \omega) = \frac{1}{N+1-r} \sum_{i=0}^{N+1-r} p_1(\vec{x}, t_i, \omega) p_2(\vec{x} + \vec{\xi}, t_i + r\tau^1 \omega) \qquad (2)$$

where $r = 0, 1, 2, 3, \ldots m$, $\tau = r\tau^1$

N + 1 equals the number of data samples (digital bits) taken for each record in a period of time T, and was limited by the sampling rate of the equipment and the core storage. For this study, the sampling rate was 8000 samples/sec per channel (16 000 samples/sec total), and the total core storage, being limited to 15 000 samples, dictated slightly less than 1 sec for the record length T. The space time cross-correlation of equation 2 indicates the statistical similarity between the pressure signatures at $\vec{x}$ and $\vec{x} + \vec{\xi}$ for each incremental time delay τ over the range m (the total number of lags used). If a statistically similar pressure signature was therefore observed at two spatial locations, but at different times, the cross-correlations detected this. Filtering the data before performing the calculations permitted examination of a frequency-limited pressure signature.

The data used in this study were acquired in a thin or relatively small dimensional scale boundary layer. Consequently, the spectrum distribution of the energy showed a wide range of frequencies containing major contributions. The frequency range of the data examined, in terms of a Strouhal-type number, was approximately $0.002 \leq \omega\theta/U_\infty \leq 0.2$.

To survey this wide frequency range required playback tape speed reduction in some cases. By this technique a sampling rate of 8000 samples/sec and corresponding Nyquist frequency of 4000 Hz was extended to an effective rate of 32,000 samples/sec or a Nyquist frequency of 16,000 Hz (when one-quarter of the original tape speed was used). This upper frequency limit is probably comparable to about 2,000 Hz for large-diameter supersonic vehicles.

3.5 Error Discussions

In this section, general sources for possible error in the correlation calculations are considered and assessed. Some of these errors are unique to correlation studies. The methods utilized to determine their magnitude are described in detail, and values for the errors are given where practical. Detailed quantitative corrections applied to every cross-correlation are omitted for the sake of brevity.

3.5.1 Error due to system noise--Noise due to data reduction system electronics can enter either before or after filtering. Noise introduced before filtering could conceivably be correlated and would thereby tend to bias the phase information. If, however, the noise were uncorrelated, it would tend to affect only the normalization process by an additive factor. The result of such a normalizing error would be to scatter data for non-zero τ. The data for this study seem to indicate that no significant noise entered the system before the filters (every sample of data for this study was examined for noise content).

In some data, digitized at a later time than the bulk of the data, electrical noise was introduced into the signal leads prior to digitizing but after filtering. Noise thus entering the system after the filter can affect the normalization in two ways. Assuming the noise was broad band with a flat spectrum, it would appear in the autocorrelations as a sharp peak at $\tau = 0$. If it were correlated between channels, it could also produce a sharp peak at $\tau = 0$ in the cross-correlations. The data for M3.48 aft-facing step and M3.45 undisturbed flow indicated that significant uncorrelated noise entered the system after the filters. The pertinent calculations performed to correct for this undesirable noise are shown for narrow band data and broad band white noise.

The unnormalized autocorrelation is the Fourier transform of the PSD and can be written

$$A'(\tau) = \int_0^\infty \mathrm{PSD}(\omega) \cos \omega\tau \, d\omega = \int_0^{\omega_c} P_2 \cos \omega\tau \, d\omega + \int_{\omega_0-\Delta/2}^{\omega_0+\Delta/2} P_1 \cos \omega\tau \, d\omega \qquad (3)$$

where P_2 is the amplitude of the noise PSD (assumed constant) and P_1 is the amplitude of the filtered signal

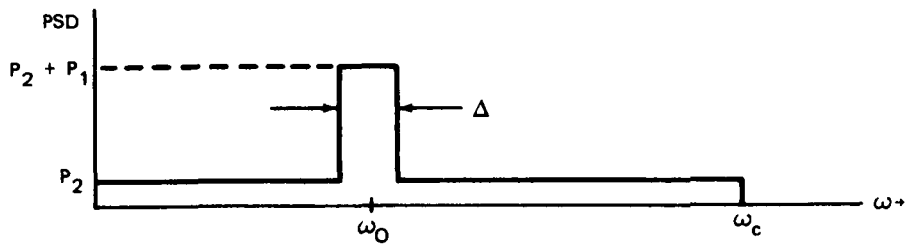

Thus

$$A'(\tau) = P_2\omega_c \frac{\sin \omega_c\tau}{\omega_c\tau} + P_1 \Delta/2 \frac{\left[\sin(\omega_c + \Delta/2)\tau - \sin(\omega_0 - \Delta/2)\tau\right]}{(\Delta/2)\tau}$$

$$= P_2\omega_c \frac{\sin \omega_c\tau}{\omega_c\tau} + P_1\Delta \frac{\sin(\Delta/2)\tau}{(\Delta/2)\tau} \cos \omega_0\tau \qquad (4)$$

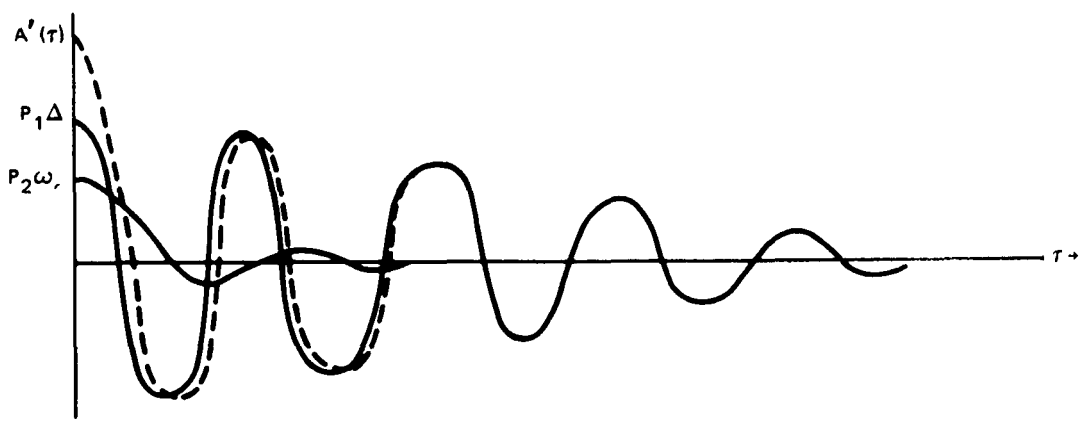

Here, the solid lines represent the two contributing parts of the signal, and the dashed line their sum. Normalization factors for the cross-correlation are determined by A'(0) which is exactly where the broadband noise has its greatest effect

$$A'(0) = P_2\omega_c + P_1\Delta \qquad (5)$$

The cross-correlations performed on those data where significant amounts of noise were present were corrected by one of the following two methods. The first method was to estimate the level of white noise from the PSD's and then compute its contribution to the mean square by integrating over all frequencies. This level was then subtracted from the overall level computed by the digital program giving the mean square level of the signal. The square root of the ratio of the overall mean square levels to the signal mean square level was then used to scale the normalized cross-correlation. Mathematically this was as follows:

Let

N = noise level = $P_2 \omega_c$

S = signal level = $P_1 \Delta$

$A'(\tau)$ = autocorrelation

$R'(\tau)$ = cross-correlation

$\overline{R}(\tau)$ = incorrectly normalized cross-correlation

$R(\tau)$ = correctly normalized cross-correlation

The data were normalized

$$\overline{R}_{12}(\tau) = \frac{R'_{12}(\tau)}{\sqrt{A'_1(0)A'_2(0)}} = \frac{R'_{12}(\tau)}{\sqrt{(N_1 + S_1)(N_2 + S_2)}} \tag{6}$$

This was then corrected by

$$R_{12}(\tau) = \frac{\sqrt{(N_1 + S_1)(N_2 + S_2)}}{\sqrt{(S_1)(S_2)}} \overline{R}_{12}(\tau) = \frac{R'_{12}(\tau)}{\sqrt{(S_1)(S_2)}} \tag{7}$$

as desired.

The second method involved visual determination of the amount of correlation due to the signal by extending the envelope of the autocorrelation to $\tau = 0$. This method was used when the PSD's were too poorly defined to use the first method.

Certainly some error is expected to be introduced due to error in estimation of the signal-to-overall-noise ratio, especially in cases where the noise level is high. This may explain some of the scatter in data from the flows indicated above.

3.5.2 Phase error.--The phase error introduced by electronic devices or by mechanical tolerances in both data acquisition and data reduction equipment were checked carefully throughout the frequency range of interest for this study. By means of simultaneously sensed sine waves, comparative end-to-end phase checks were made, from just behind the transducer in the data acquisition system to just in front of the digitizer in the data reduction circuit. Because these prerecorded sine waves were spaced throughout the frequency domain, the characteristics over small frequency ranges in the narrow band filters were checked with sine sweeps. In all cases, phase errors were constrained to less than 10°. This was accomplished by restricting the frequency range, choosing different filters (by changing the tape speed, a particular narrow band of frequencies could be examined at different fixed-filter settings), or by eliminating certain data from analysis. The only exception to this was in the case of some data recorded on a tape transport with a skewed record head. The amount and direction of skewness were accurately determined by the fixed time delays (or variable phase with frequency). The time delay for each pair of heads and playback speed was determined, and corrections were made on the time axis of each cross-correlation to account for the difficulty.

The error in the time domain of the cross-correlation due to phase error between recording channels is the period of the phase error (less than 10°) at the frequency examined. The resultant erroneous time periods for this study were small compared to one lag, and hence negligible.

3.5.3 Statistical error discussion.--All of the data from this study may be presented in either of two ways: they may be presented in terms of correlation functions, or in terms of cross-spectral density functions. The two are Fourier transform pairs. Hence, the statistical errors in the correlation functions can be related to those in the cross-spectral density functions.

An important parameter for determining the statistical error is the BT number which is the product of the resolution bandwidth (B) and the record length (T). The 90% confidence levels for the cross PSD's are determined from the relation $\Delta dB \simeq (200/BT)^{1/2}$ (ref. 5). This means 90% of all the data points will fall between log (P_o) + $\Delta dB/10$ and log (P_o) - $\Delta dB/10$ where P_o is the true PSD plotted on a log scale.

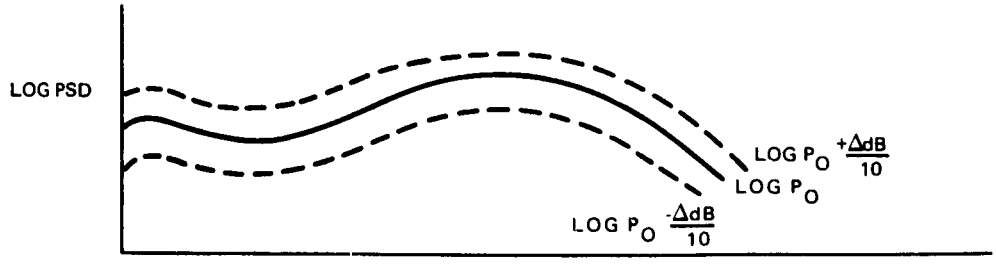

In terms of a linear scale, letting $\Delta dB = 10 \log \epsilon$, the 90% confidence curves are ϵP_o and $1/\epsilon P_o$. Then 90% of the points will have an error of less than $(\epsilon - 1) \times 100\%$.

To minimize error (obtain the narrowest confidence bands), the record time and the bandwidth should be maximized. However, increasing the bandwidth decreases the information in the frequency domain because it averages over all the frequencies in the band. This suggests choosing a very long record length so accuracy and resolution could both be maintained. Unfortunately, record length is limited in this study because of two major factors: (1) the blowdown wind tunnel characteristics are not stationary for long periods of time, and (2) long time records are not practical on the digital computer which has a fixed storage capacity (in this case, approximately 15,000 bits total).

In digital cross-correlation analysis, the sampling rate is related to the record time and the number of samples by:

$$\text{Samples} = \text{sampling rate} \times \text{record length} \tag{8}$$

In addition the sampling rate is related to the Nyquist frequency by:

$$\text{Nyquist frequency} = 1/2 \text{ sampling rate} \tag{9}$$

The Nyquist frequency is the maximum frequency that can be distinguished from lower harmonics. To avoid the presence of higher frequencies, a low-pass filter is utilized to permit attenuation of all frequencies above the Nyquist frequency. This filter is always placed in the circuit prior to digitizing to avoid fold-back (the incorrect interpretation of high-frequency information as low-frequency data). For reasonable definition of a spectrum, it is desirable to have the Nyquist frequency much larger than the resolution bandwidth. Hence, for a fixed number of samples, the record time decreases as the Nyquist frequency or the sampling rate increases.

The number of lags and the lag time are variables associated with definition of the correlation functions. They are related to the other variables by

$$\text{Incremental lag time} = \frac{1}{\text{sampling rate}} \tag{10}$$

and

$$\text{Total number of lags} = \frac{\text{sampling rate}}{\text{resolution bandwidth}} \tag{11}$$

The variables of interest are presented for each of the methods in table 2. Methods 1, 2, and 3 were used for broad band analysis during a previous study. The large statistical scatter in the broad band analyses makes it difficult to estimate narrow band relationships directly from those data. Methods 4 through 6 were used for narrow band analysis of forward-facing step, aft-facing step at M1.41, and shock-disturbed flow, while 7 through 9 were used for narrow band analysis of undisturbed flow and aft-facing step at 3.48. Method 10 was included to get better definition in the time domain at the expense of bandwidth resolution, but was actually not used for data analysis. It should be noted that the large range of variables results from two major factors – flexibility in both sampling rate (by means of tape speed reductions as well as variable sampling rates), and choice of total number of lags.

TABLE 2

STATISTICAL ERROR DATA

Method No.	1	2	3	4	5	6	7	8	9	10
Sampling rate $\left(\frac{\text{samples}}{\text{sec}}\right)$	40 000	40 000	40 000	5 000	10 000	40 000	8 000	16 000	64 000	64 000
Nyquist frequency (Hz)	16 000	16 000	16 000	2 500	5 000	20 000	4 000	8 000	32 000	32 000
Lag time (μsec)	25	25	25	200	100	25	125	62.5	15.625	15.625
No. of data bits per channel	8 800	8 800	8 800	7 440	7 440	7 440	7 440	7 440	7 440	7 440
Record length (sec) (real time)	0.22	0.22	0.22	1.488	0.744	0.186	0.930	0.465	0.116	0.116
Resolution bandwidth (Hz)	320	160	80	50	100	400	80	160	640	512
Total no. of lags	125	250	500	100	100	100	100	100	100	125
BT number	70.4	35.2	17.6	74.4	74.4	74.4	74.4	74.4	74.4	59.4
ΔdB	1.69	2.38	3.37	1.64	1.64	1.64	1.64	1.64	1.64	1.83
ϵ	1.47	1.73	2.17	1.46	1.46	1.46	1.46	1.46	1.46	1.53
Possible error (%)	47	73	117	46	46	46	46	46	46	53

Large statistical variances in cross-power spectral densities do not imply the same variance for all regions of the cross-correlations. In fact, the error tends to be least at the cross-correlation peak and greatest for times far from the peak. The error in the peak is the error in the mean square value. For narrow band data, this can be estimated by replacing the resolution bandwidth by the data bandwidth (assuming the band is sufficiently narrow to consider the PSD flat and the system nondispersive). For the 1/3-octave band filters utilized during this narrow band study, the pertinent variables are presented in table 3.

TABLE 3
NARROW BAND STATISTICAL ERROR DATA

Method No.	4	5	6	7	8	9	10
Record length (sec)	1.488	0.744	0.186	0.930	0.465	0.116	0.116
Frequencies (Hz)	800	3 200	12 800	800	3 200	12 800	800
1/3-octave bandwidth (Hz)	185	741	2 965	185	741	2 965	185
BT number	275	551	551	172	344	344	21
ΔdB	0.853	0.602	0.602	1.078	0.762	0.762	3.09
ϵ	1.22	1.15	1.15	1.28	1.19	1.19	2.04
Error (%)	22	15	15	28	19	19	104

The large expected error in row 10 suggested that those data not be used. Therefore, those data were used only qualitatively in description of system noise. Method 7 (800 Hz data) indicates that some of the scatter may be due to statistical variations caused by core storage limitations.

It should be noted that filtering of the data, although not absolutely essential for the description of narrow band phenomena, increases the statistical accuracy of the data in a convenient manner.

3.5.4 Data interpolation errors.--Cross-correlation values are computed in the time domain at only a finite number of time separations (multiples of the incremental lag time). Intermediate values must be interpolated. Since the characteristic oscillation frequency for narrow band cross-correlations of data is the geometrical center frequency, the number of points for each narrow band cycle depends on the definition in the time domain. Typically, for the narrow band data of this study, the number of points per cycle varied from 3 to 10. Interpolation is more accurate when the number of points is increased or when the curve's shape is known.

Conclusions based on data with only 3 points is undoubtedly less accurate than those based on 10. The maximum error for this aspect of data interpretation occurred for forward-facing step, aft-facing step at M1.41, and shock-disturbed flow data in the two highest bands of frequency. Although knowledge

of the curve's shape reduces the error from this source, some of the data scatter may be due to interpolation error.

3.5.5 Sources for false correlation.--One source of bias error is the possible introduction of a false correlation due to the filter bandwidths becoming too small. The extent of this error can be estimated theoretically or determined experimentally. On the basis of an empirical study in which the filtered signals from two completely uncorrelated random-signal generators were compared, it was determined that, at frequencies lower than 100 Hz, an octave band or more of frequencies should be examined, but above this, 1/3-octave bands or less could be used. The bias error introduced by this effect was always negligible (2.5% or less) in this study.

"Correlation noise," a term used to signify an unwanted indication of correlation, was more troublesome than error from filter width. Such "noise" is always present in correlation analysis, and is due to replacing the integration process by a summation. The time-averaging (time-smearing) effect provides enough statistical similarity that this "correlation noise" falsely indicates some correlation between uncorrelated signals. For this study, this "correlation noise" appeared as a normalized correlation level of about 0.05 for all times. Therefore, values of this order were not used.

4. RESULTS FROM SUPERSONIC FLOW

In this section, the results of calculations performed on the data are presented graphically or numerically. Pertinent comments are included where required. The bulk of the discussion concerning interpretation or comparison with theory is to be found in section 5. The reader is advised to consult the discussions prior to interpolation or extrapolation of this section's content.

The data are presented in three forms. First, they are presented as approximate contours of equal correlation in the $\xi_x \xi_z$ plane (plane of the surface) at $\tau = 0$. These contours are extrapolated from data parallel, at 30°, at 60°, and perpendicular to the direction of flow. Approximate volumes under these correlation surfaces were obtained, and are presented as an effective area of unit (perfect) correlation and an approximate rectangular shape. The length and width of a panel over which greatest pressure cancellation occurred (at $\tau = 0$) are also presented. It should be remembered, however, that time-varying effects such as coincidence may negate the usefullness of sizing to these dimensions. Also, even if maximum pressure-cancellation is achieved for one mode, another mode may be strongly excited.

Second, data are presented as decay curves. These are the peak correlation values for any particular separation distance plotted as a function of separation. These curves have been assumed to be approximately exponential, and an exponential decay has been fitted for each set of data.

The third method of data presentation is a plot of the relationship of separation distance and time displacement at which peak correlation occurs. The slope of this curve gives the convection velocity.

4.1 Undisturbed Flow

Contours of equal correlation coefficient for the three 1/3-octave bands of data examined in detail (whose geometrical mean-frequencies were $\omega\theta/U_\infty = 0.01$, 0.04, and 0.16) are given in fig. 1. Equivalent square areas of perfect correlation in the plane of the surface have been calculated for each and are given as $\Lambda_{xy}/\theta^2 = 1830$, 1660, and 89 respectively. Unfortunately, due to the nonlinear frequency dependence of the data, interpolation between them is not possible. This inability to interpolate makes application of these data more difficult. Actually, the undisturbed flow dependence on frequency is more well-behaved than disturbed flows examined, and in that sense, lends itself better to an assumed distribution with frequency based on coherency considerations. The area seems to be a continuously varying (decreasing) function with frequency, but further definition is required to indicate the exact dependence. However, even if one were to attempt such a definition, the variable of Mach number would then have to be introduced as a possible influence on the results. Considering that the undisturbed flow

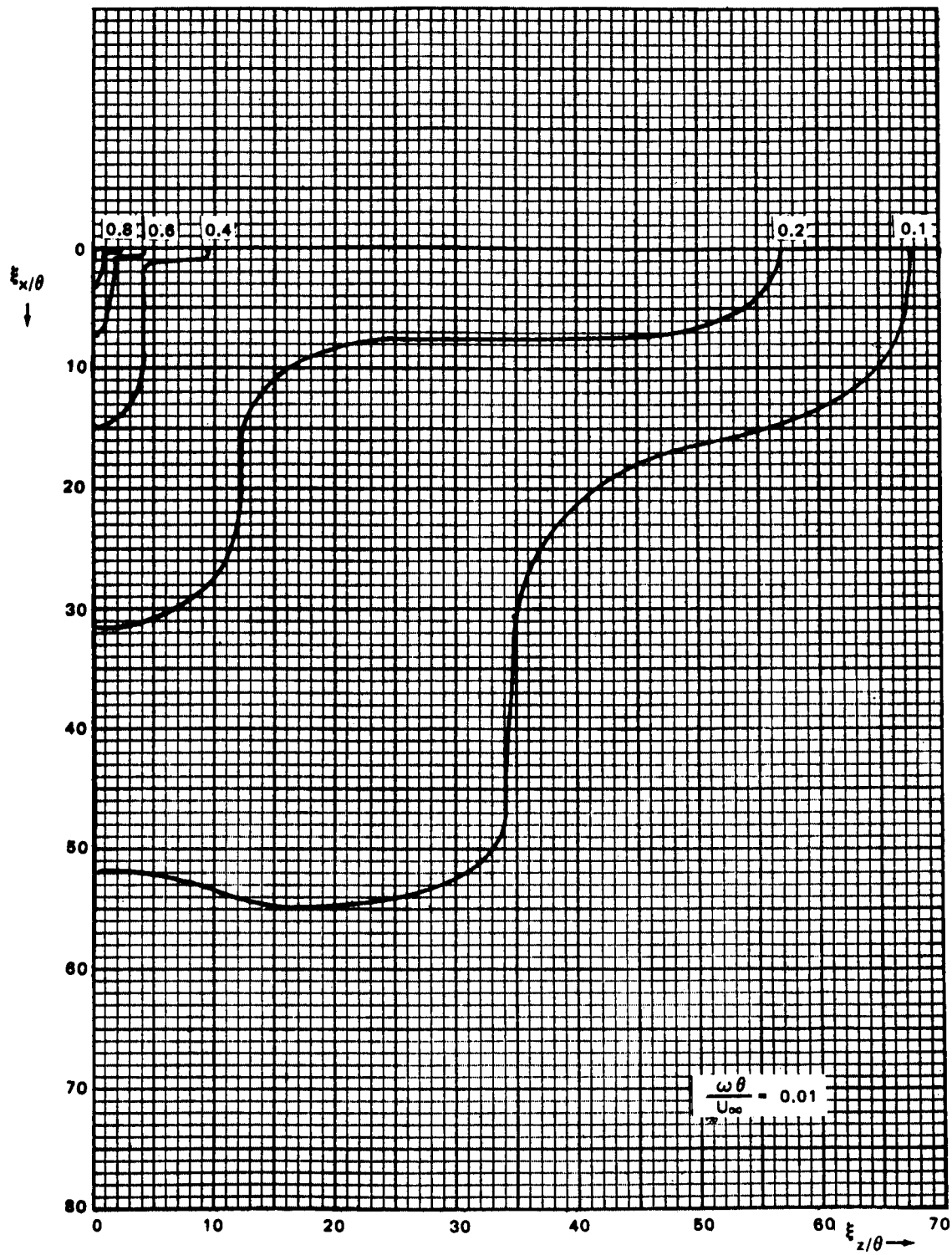

Figure 1. Contours of Equal Correlation Coefficient, Undisturbed Flow, M 3.45. - Page 1 of 2

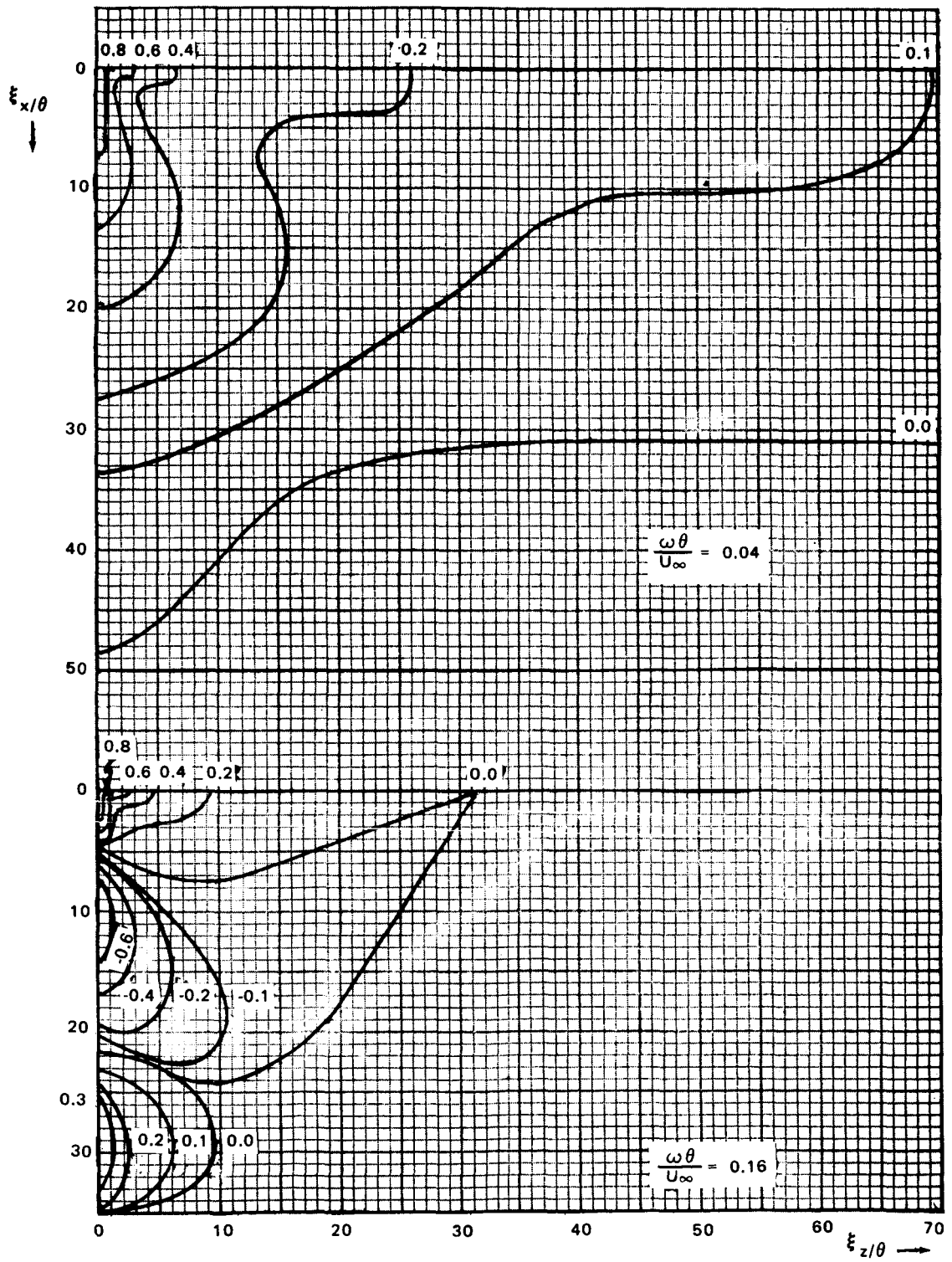

Figure 1. - Concluded

has the most uniform distribution with frequency, it is easy to understand the difficulty in describing the frequency dependencies of disturbed flow. Additional detailed discussions of these aspects are contained in section 5.

In previously documented studies, the results have been presented as separated in the time and space domains for the frame of reference moving with the boundary layer. In that method, the decay of the maxima was given as a function of time delay τ. The results of this study have indicated that separability does not exist in that frame. Section 5 discusses this more fully. What has resulted from the further work presented here is that the decay in the spatial separation plane (rather than the time plane), and the convection velocities, completely describe the "separable" functions. In light of these results, the spatial decay for the three 1/3-octave bands examined are presented in figure 2 versus spatial separation. The reader must make careful note, however, that interpolation between these curves can not be made. This is due (as mentioned above and described in detail in par. 5.3) to the variability of decay rate with frequency.

The convection velocity was found to be nondispersive (not frequency-dependent) within the accuracy of the data. However, detailed narrow band analysis provided the basis for a better interpretation of this variable. For close separation, the convection velocity is not a constant. It increases rapidly as separation distances are increased, until it finally becomes asymptotic to a value of $U_c = 0.94\ U_\infty$ for M3.5 (as previously quoted). A plot of the nondimensionalized τ_o versus ξ_x (the slope of which gives the convection velocity) is given in figure 3. Interestingly enough, if it is assumed that there is some preferred eddy size (or vortex size) which predominates the correlation, the maximum coherency or frequency at which the narrow band cross-correlation maximizes in conjunction with the convection velocity should give some estimate of its relative size (since $\omega/U_c = k$ where k is the wave number and hence inversely proportional to a length dimension). The results for M3.5 undisturbed flow could be caused by an eddy (or vortex) which stretches to nearly four times its original size while going from its origin to its final location at the outer fringes of the boundary layer.

4.2 Aft-Facing Steps

Prior to the planning of the experimental acquisition of data on which this narrow band analysis study is based, little was known of the peculiarities associated with FPL's in disturbed flow. Now that a study of this sort has been performed, enough new knowledge exists to allow a better investigation of certain phenomena. For example, the region directly behind the step has low-level fluctuating pressures, predominated by a low-frequency phenomenon. The region of reattachment well downstream of the step is of more vital interest from a structural design point-of-view because of its considerably higher levels, with energy more uniformly spread throughout the frequency range. The results of this study suggest that the correlation properties of the FPL's are quite different beyond reattachment (on the basis of the correlation in the direction of the flow). Unfortunately, however, without the advantage of this prior knowledge, the base region of the aft-facing step (within the separated flow) is the only region for which data were taken extensively for this disturbed flow geometry. The rest of this section will therefore describe in detail the aspects learned about this base region.

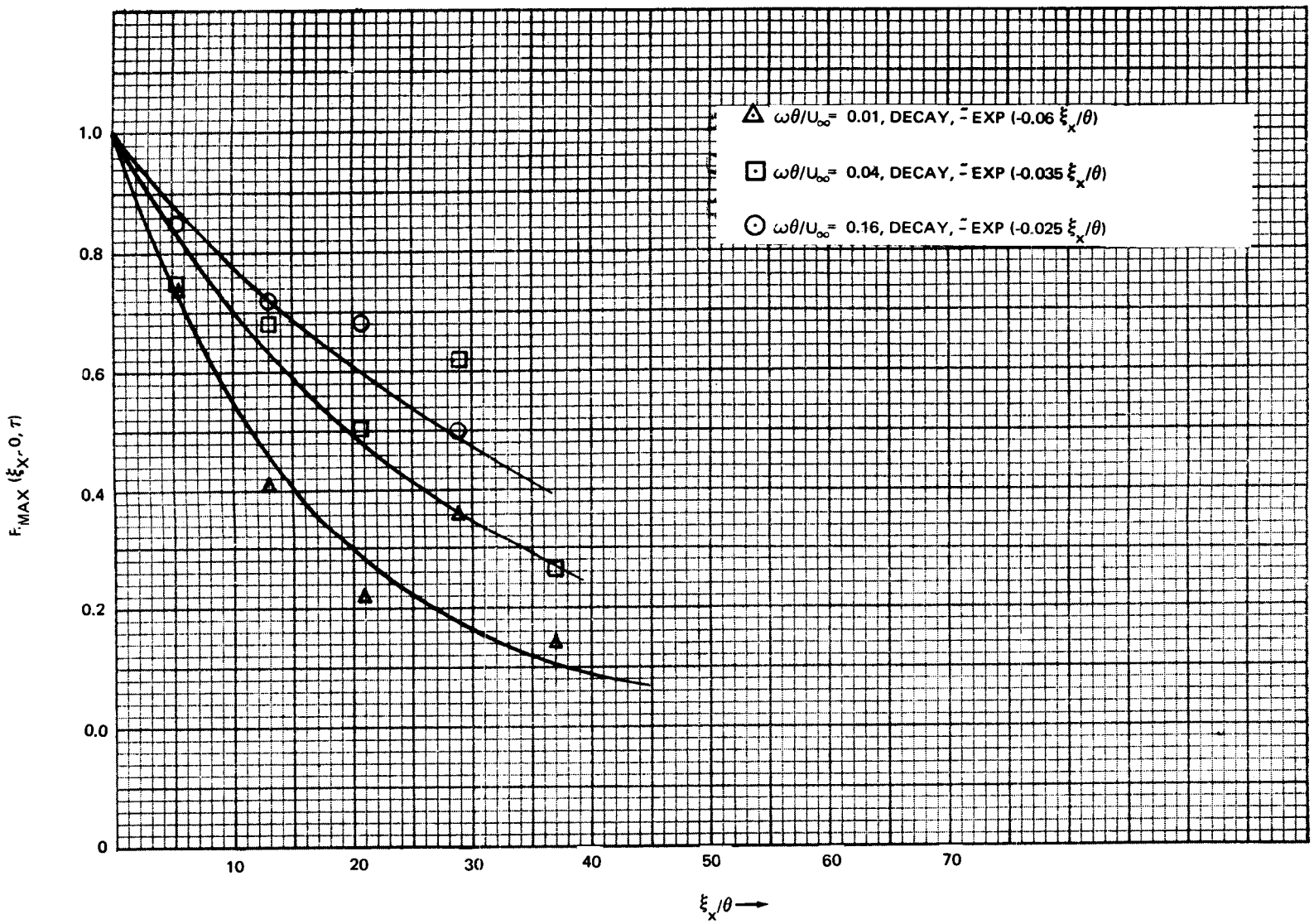

Figure 2. Spatial Decay of the Cross-Correlation Maxima for Undisturbed Flow FPL's, M 3.45.

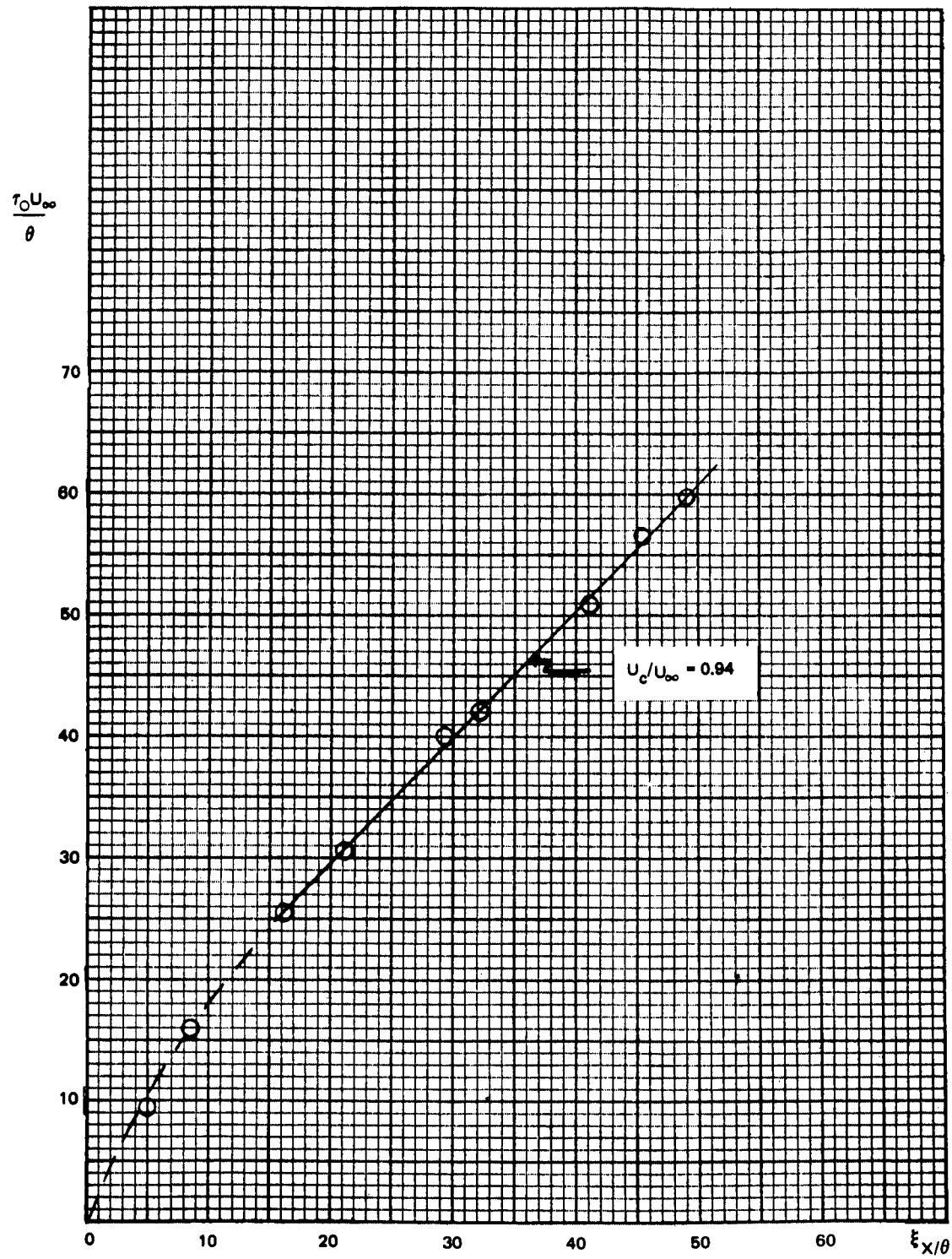

Figure 3. Convection Time Vs. Spatial Separation at M 3.45.

As reported in reference 1, a strong lateral convection (perpendicular to the flow) velocity was observed near the aft-facing step face. Narrow band cross-correlation permitted closer examination of this phenomenon. It was determined that the phenomenon has to do with some kind of pressure source moving in a direction perpendicular to the boundary layer. Some of the observations are summarized below:

(1) Maximum coherency is in the same narrow band of frequencies at which the psd peak occurs ($\omega\theta/U_\infty \simeq 0.01$) for both M1.41 and M3.48.

(2) The velocity of propagation along the step face perpendicular to the flow is on the order of 0.15 to 0.3 of the free-stream velocity.

(3) The resultant velocity vector which generates the appropriate velocities measured in the two perpendicular directions x and z was $0.44\ U_\infty$ at both Mach numbers and at an angle (assuming a straight line between the points) of $-13.8\ M_\infty^0 + 90°$ with the flow. Surprisingly enough, the line going through the two points intersected 90° at zero Mach number (as indicated by the equation). One explanation might be a flow phenomenon which "peels" off the top edge of the step at some angle, depending on the flow speed.

(4) The spatial correlation contours show decided elongations in the direction of propagation of this phenomenon.

To identify the source of this peculiarity, several factors were considered. First, if it was an acoustical source, the speed of sound should have been observable in either a direction perpendicular to the flow or at some other angle in the region of trapped recirculating air. By checking the two Mach numbers available, it was definitely not identifiable as sound waves for M1.41, but coincidentally could have been at M3.48. Reference 6 was examined, assuming some sort of cavity phenomenon where the flow tranversed an opening of a triangular-shaped finite cavity. However, the authors of that paper concluded on page 99 that, "on the basis of experimental evidence, transverse modes are not normally excited."

If an edgetone-like feedback system existed, the frequency should have been proportional to some wavelength times a velocity divided by the distance between the edge and the flow source. If the two walls at fixed distances were involved, the frequency should have changed because the velocity changes. If the flow over the aft-facing step edge and the location of reattachment were the source and edge respectively, the frequency should have changed due to the shortening of the separated flow extent with Mach numbers. Since the frequency did not change, neither of these explanations is suggested.

Another possibility is a vortex shedding off the top edge of the step. Such a possibility would permit the velocity to be Mach number-dependent, and the frequency to be dependent on geometry (constant frequency). It is certainly of interest to investigate the existence and sources of such an FPL in terms of other geometries for aft-facing steps: for example, different step heights, or a three-dimensional, axially symmetric model on which no physical restrictions exist in the z direction (perpendicular to the flow).

The broad band results quoted in reference 1 indicated a convection velocity that was very high (approximately equal to the free-stream velocity) in the z direction. The results of this narrow band analysis indicate that the actual velocity of the phenomenon in the z direction is quite low. However, if the average is taken over all frequencies, the trace velocity for the high frequencies ($\omega\theta/U_\infty = 0.16$) are as much as 10 times the free-stream velocity in the z direction. This is what would occur if the trace velocity approached infinity for the frequencies not affected by a phenomenon moving to the side, since they would only have a velocity in the x direction. Hence, the broad-band average gave an incorrect illusion of very high lateral convection velocities.

With the obvious predominence of this low-frequency source moving perpendicular to the flow near the step face, all the results from this study for aft-facing steps must be considered as strongly influenced by it. Hence, the correlation properties cannot be assumed equivalent to those under, or downstream of, reattachment. However, if such a source ordinarily exists behind aft-facing steps, the results presented here could be representative of this phenomenon. Figures 4 and 5 show the correlation coefficients in contours of equal values. Figures 6 and 7 show the spatial decay of the maxima for the three narrow bands examined. The decay curves do not show a consistant trend with frequency but seem to indicate a more rapid decay with increasing Mach number. In paragraph 5.3, a more complete discussion is given concerning the frequency dependence for disturbed flow. It is clear from that discussion, that examining three widely separated narrow bands of data will not necessarily convey a clear picture of the frequency dependence unless the coherency remains invariant with spatial separation and Mach number for each disturbed flow phenomenon. With the limited data available in this study, and the inherent statistical scatter, such an assumption of invariance is neither substantiated nor disproved. The convection velocities for all frequencies examined downstream of reattachment proved to be constant after a spatial separation of $\xi_x/\theta \simeq 12$, at $0.645\ U_\infty$ for M1.41 and $0.4\ U_\infty$ for M3.48 as shown in figure 8. However, no attempt has been made to relate these convection velocities to the true boundary layer velocities before and after reattachment, these being different from U_∞. A decided kink in the convection velocity versus spatial separation at $\xi_x/\theta \simeq 12$ might be explained by the same sort of eruption process source downstream of reattachment as is in evidence for undisturbed flow; i.e., the predominant source is generated, quickly moves to a different strata of the boundary layer during which time it loses a great deal of its identity, and then continues downstream at a fixed velocity, retaining residues of its original identity for long periods of time.

Assuming symmetry in two quadrants, equivalent rectangular areas over which it can be assumed that perfect correlation exists are:

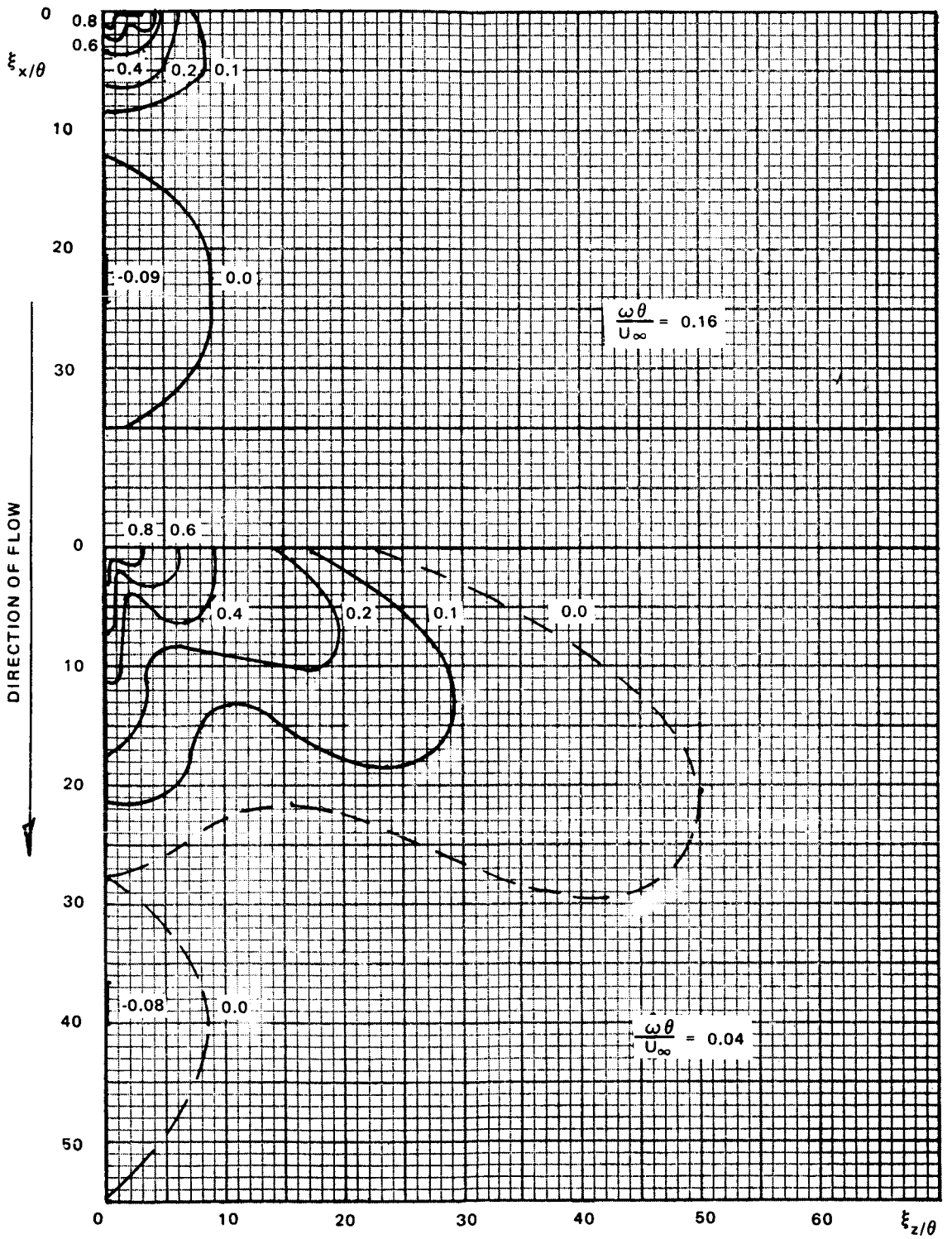

Figure 4. Contours of Equal Correlation Coefficient, Aft-Facing Step Near Face, M 3.48

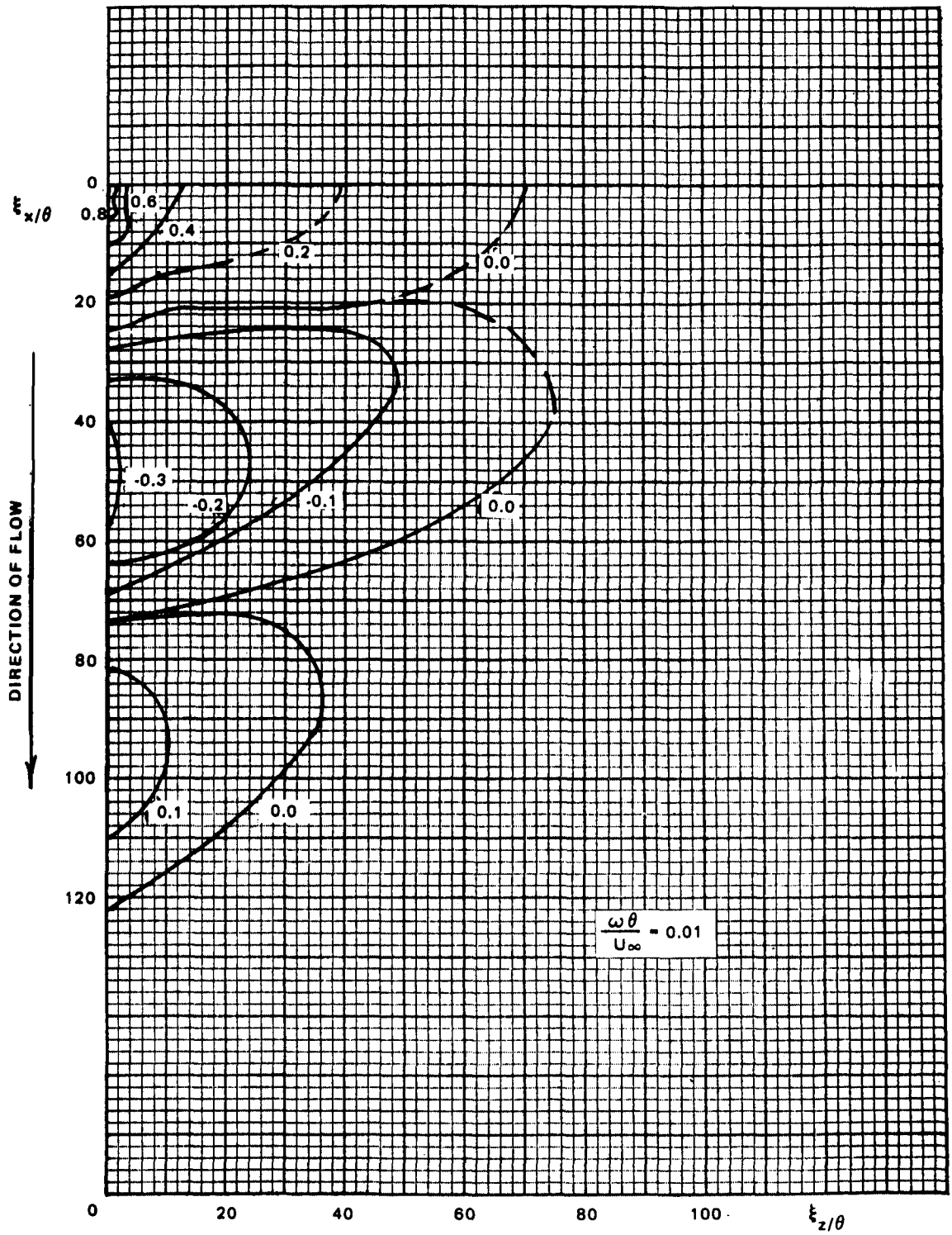

Figure 5. Contours of Equal Correlation Coefficients, Aft-Facing Step Near Face, M 1.41.

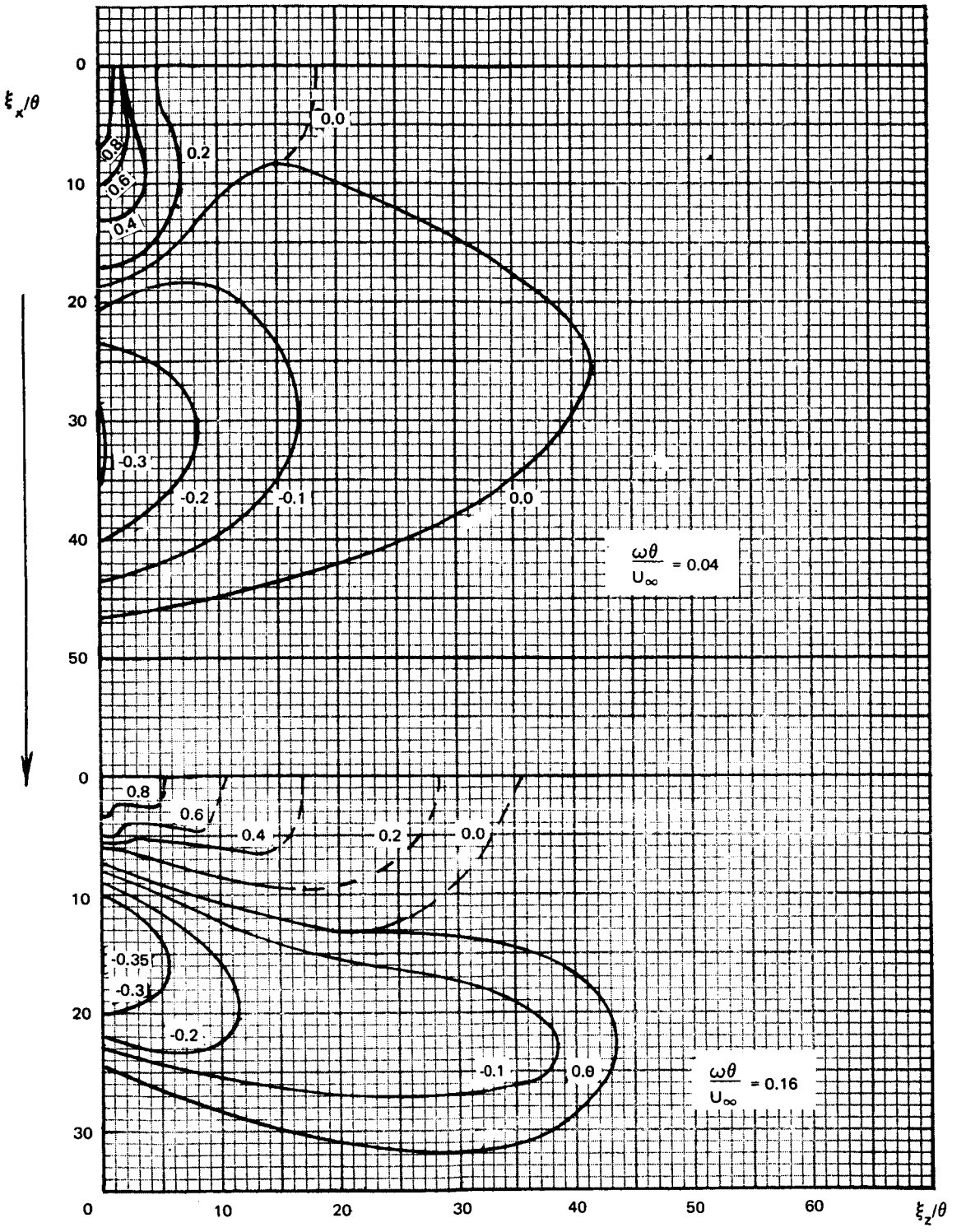

Figure 5. Concluded

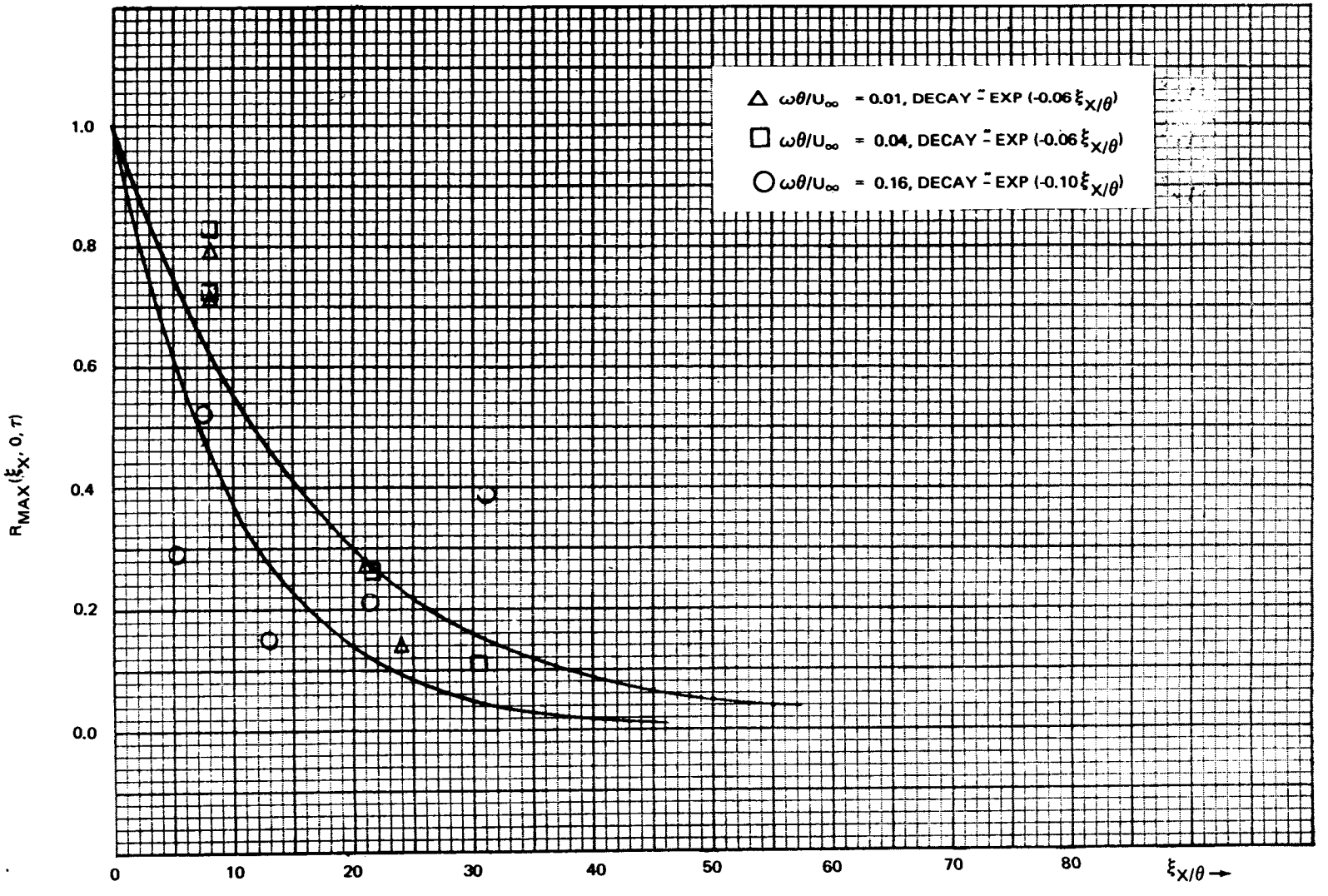

Figure 6. Spatial Decay of the Cross-Correlation Maxima for Aft-Facing Step Near Step Face, M 3.48.

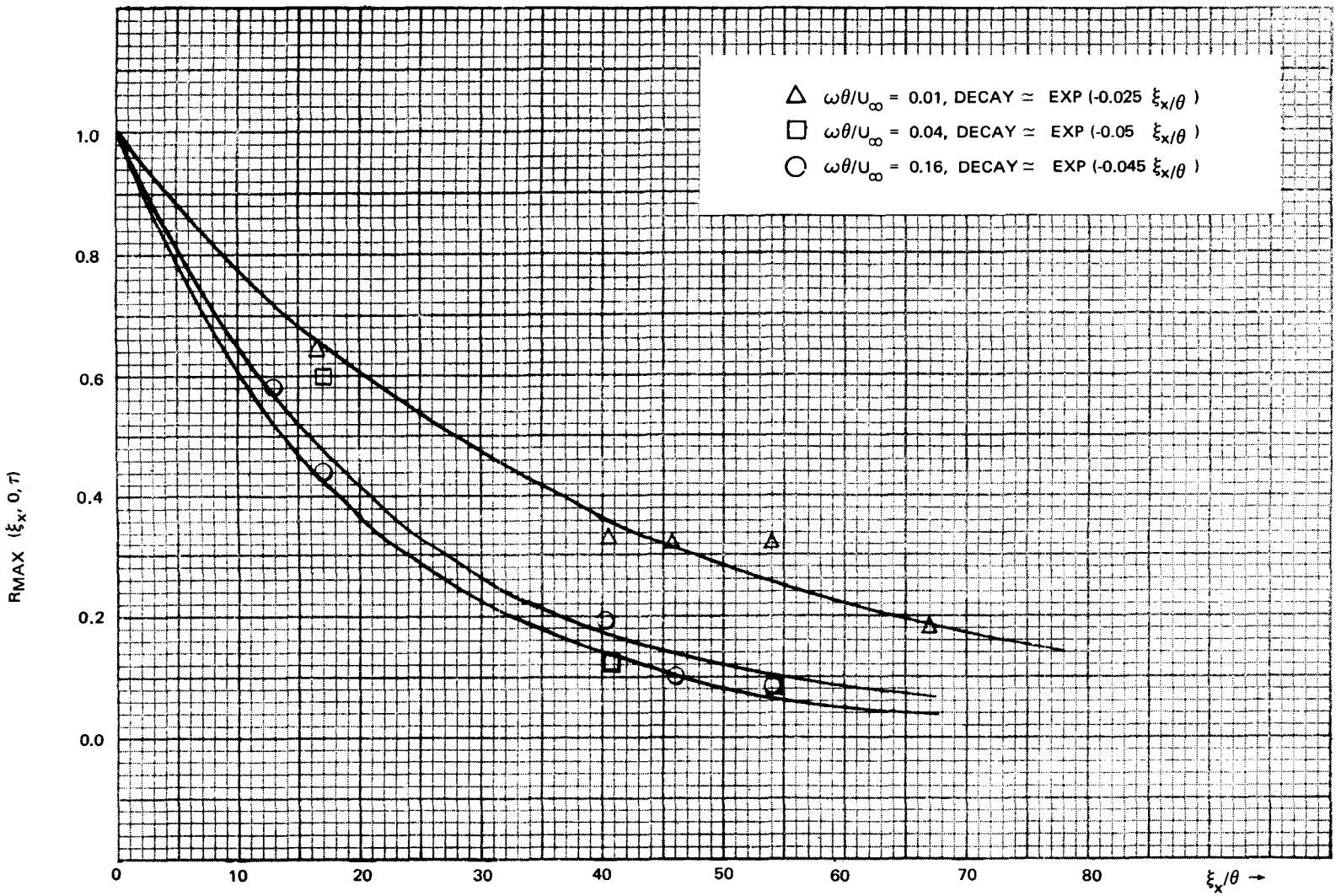

Figure 7. Spatial Decay of the Cross-Correlation Maxima for Aft-Facing Step Near Step Face, M 1.41.

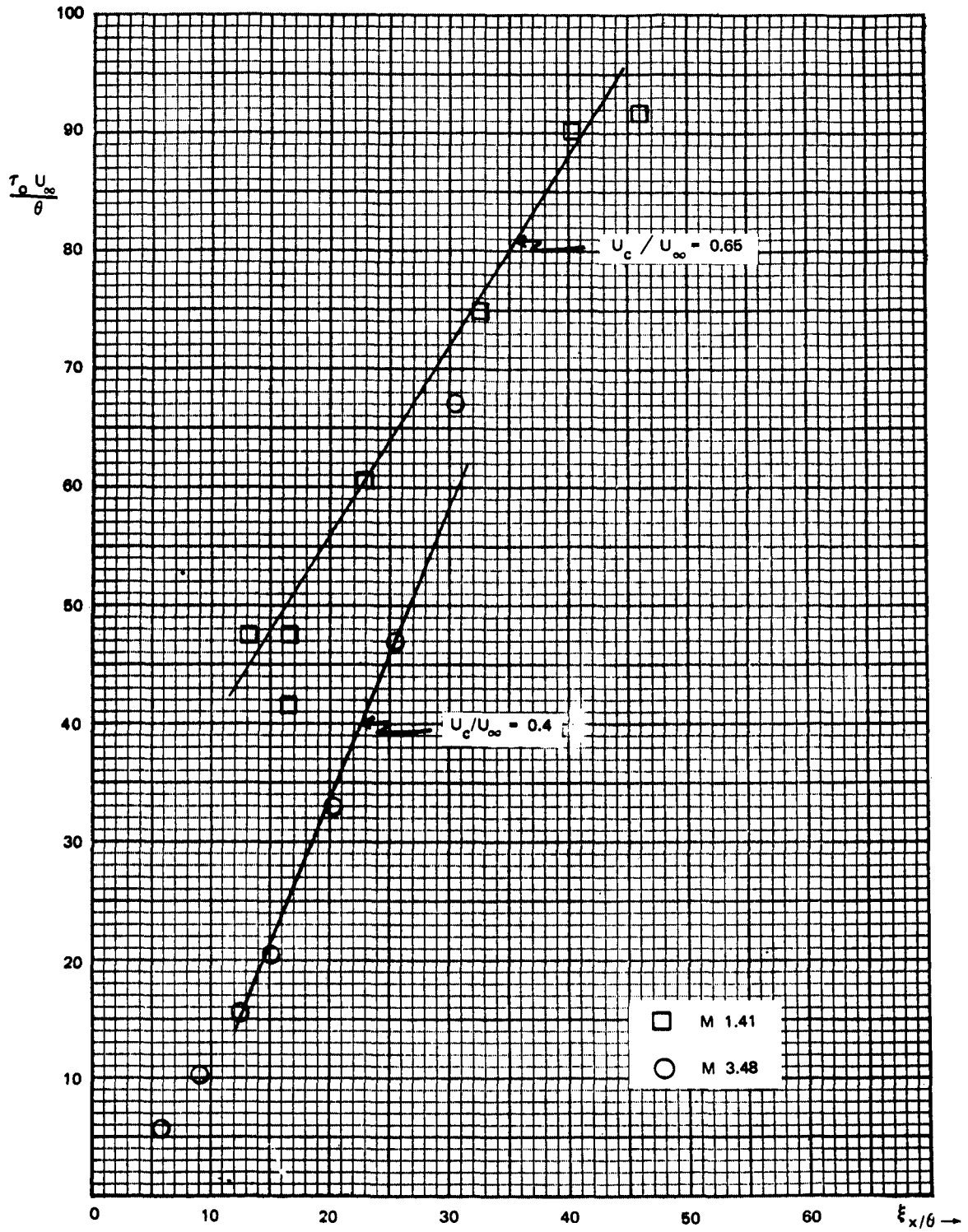

Figure 8. Convection Time Vs. Spatial Separation After Reattachment Behind Aft-Facing Steps.

$\frac{\omega\theta}{U_\infty}$		M 1.41	Approximate (L/W)	M 3.48	Approximate (L/W)
0.01	$\frac{\Lambda_{xy}}{\theta^2} =$	815 ,	2/5	Not Available	-
0.04	$\frac{\Lambda_{xy}}{\theta^2} =$	184.5 ,	2	550	1/2
0.16	$\frac{\Lambda_{xy}}{\theta^2} =$	444 ,	1/6	56	1/2

For maximum pressure cancellation to occur in the fundamental bending mode of a structural panel, accounting for the negative lobe of the correlation coefficient, the panel dimensions should be $L/\theta = 67$, $L/W = 1.4$ for $\omega\theta/U_\infty = 0.01$ or 0.16, and $L/\theta = 40$, $L/W = 2.4$ for $\omega\theta/U_\infty = 0.04$ for M1.41. By M3.48, no significant pressure cancellation effects could be observed.

4.3 Forward-Facing Step

Of the disturbed flow phenomena investigated experimentally, the forward-facing step data are the most suitable for analysis. The data quality is good, the locations are suitable for description of characteristics of the highest pressure levels at the two-dimensional plane of the boundary, and the results are comprehensive. With all of these advantages, some aspects were still difficult to interpret, demonstrating the complexity of disturbed flow phenomena.

As an example, the low frequencies near the step face were apparently partially influenced by pressure signals carried by the reverse flow. Hence, the cross-correlations indicated a positive and negative convection velocity with the zero crossing (correlation coefficient) undoubtedly affected by the existence of two peaks on either side of $\tau = 0$. These signals are more poorly correlated, lose coherence rapidly in space, travel at similar speeds but in the opposite direction as the primary signal, are not observable in any direction other than parallel with the flow, and are restricted to the low frequencies. For these reasons, the reflected signal (or signal carried by reverse flow) data were not treated specifically in this report although they are absorbed by the overall descriptors (e.g., correlation coefficients).

The data presented for narrow band analysis of a forward-facing step are for a Mach number of 3.45. Data from aft-facing steps indicate a stretching of the surface areas over which correlation occurs when the region of

separated flow is stretched. A similar condition is expected for the forward-facing step region of separated flow. No data exists to verify this assumption, so application of these data to different Mach numbers should be done with caution until further investigation of this aspect has been accomplished.

Figure 9 shows the contours of equal correlation coefficient within the region of separated flow for the three frequency regions examined. No marked dispersive tendency was exhibited, so the slope of the curve in figure 10 shows the convection velocity for any band of frequencies within the range of this study. The constant U_c observed beyond a spatial separation of approximately $\xi_x/\theta = 8$ is equal to $0.71\ U_\infty$, but is equal to approximately $0.86\ U_2$ where U_2 is the estimated velocity of the separated boundary layer. Figure 11 shows, for purposes of comparison, the ratio of $\overline{U}_c/U_\infty$ for undisturbed supersonic flow and $\overline{U}_c/U_2$ for forward-facing step flow within the region of separation. Here, $\overline{U}_c$ is the average convection velocity for a particular separation distance calculated to be ξ_x/τ_o where ξ_x is the separation distance between measurement locations and τ_o is the time displacement at which the narrow band cross-correlation reaches a maximum. As can be seen, the comparison is very good, (considering that the value of U_2 has been estimated and could be somewhat low) suggesting that the major source for the pressure signature at the wall is the separated turbulent boundary layer.

Figure 12 presents the spatial decay of the narrow band correlation coefficients. The reader is reminded that interpolation is not possible because of the complex frequency dependence. (See par. 5.3 for further details.)

Estimates of the equivalent area rectangular over which the in-phase pressures can be assumed to be perfectly correlated have been made for all three frequency ranges. Near the step face where the pressure levels maximize, the equivalent areas have been calculated assuming symmetry in two quadrants as the following:

$$\frac{\omega\theta}{U_\infty} = 0.01,\ \Lambda_{xy} = 160\ \theta^2$$

$$\frac{\omega\theta}{U_\infty} = 0.04,\ \Lambda_{xy} = 435\ \theta^2$$

$$\frac{\omega\theta}{U_\infty} = 0.16,\ \Lambda_{xy} = 23\ \theta^2$$

In the mid- and high-frequency ranges, negative correlation coefficients imply pressure cancellation effects may occur. A study of length-to-width ratios and optimum sizing of areas to advantageously incorporate these effects in a design nomograph proved impractical. No collapse of the optimum areas was possible in disturbed flow because of the peculiar frequency dependence.

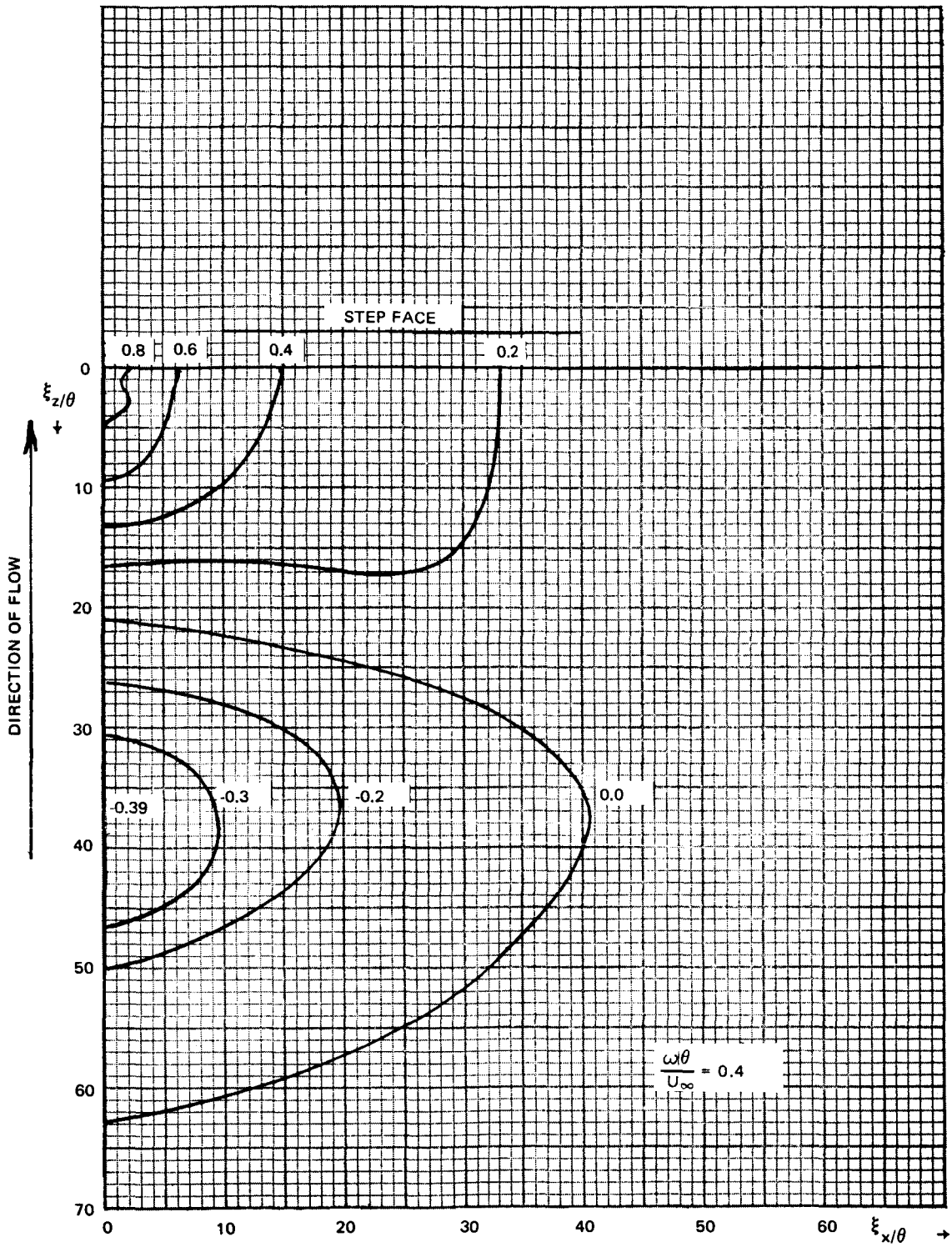

Figure 9. Contours of Equal Correlation Coefficient, Forward-Facing Step, M 3.45. - Page 1 of 2.

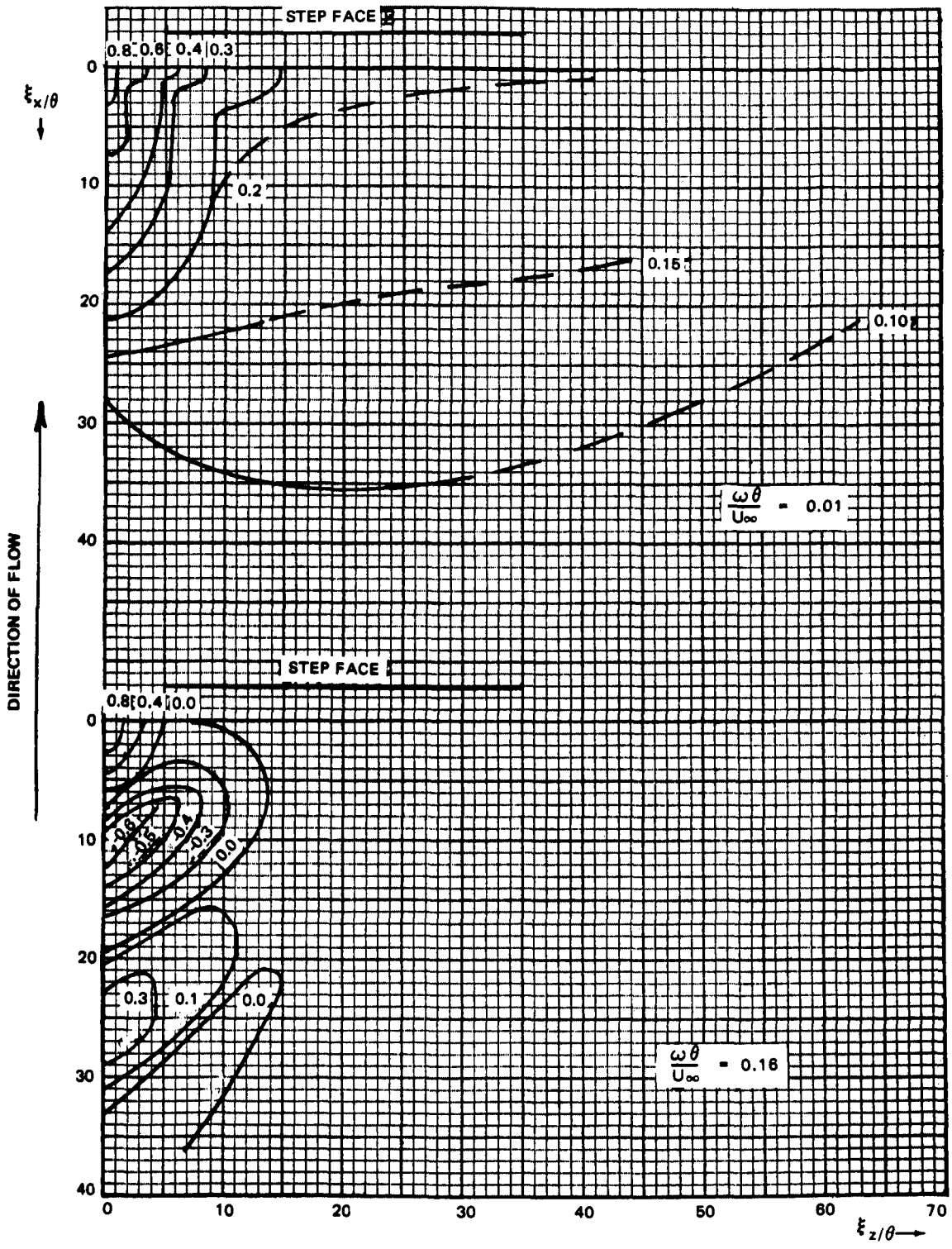

Figure 9. Contours of Equal Correlation Coefficients Forward-Facing Step, M 3.45. - Concluded

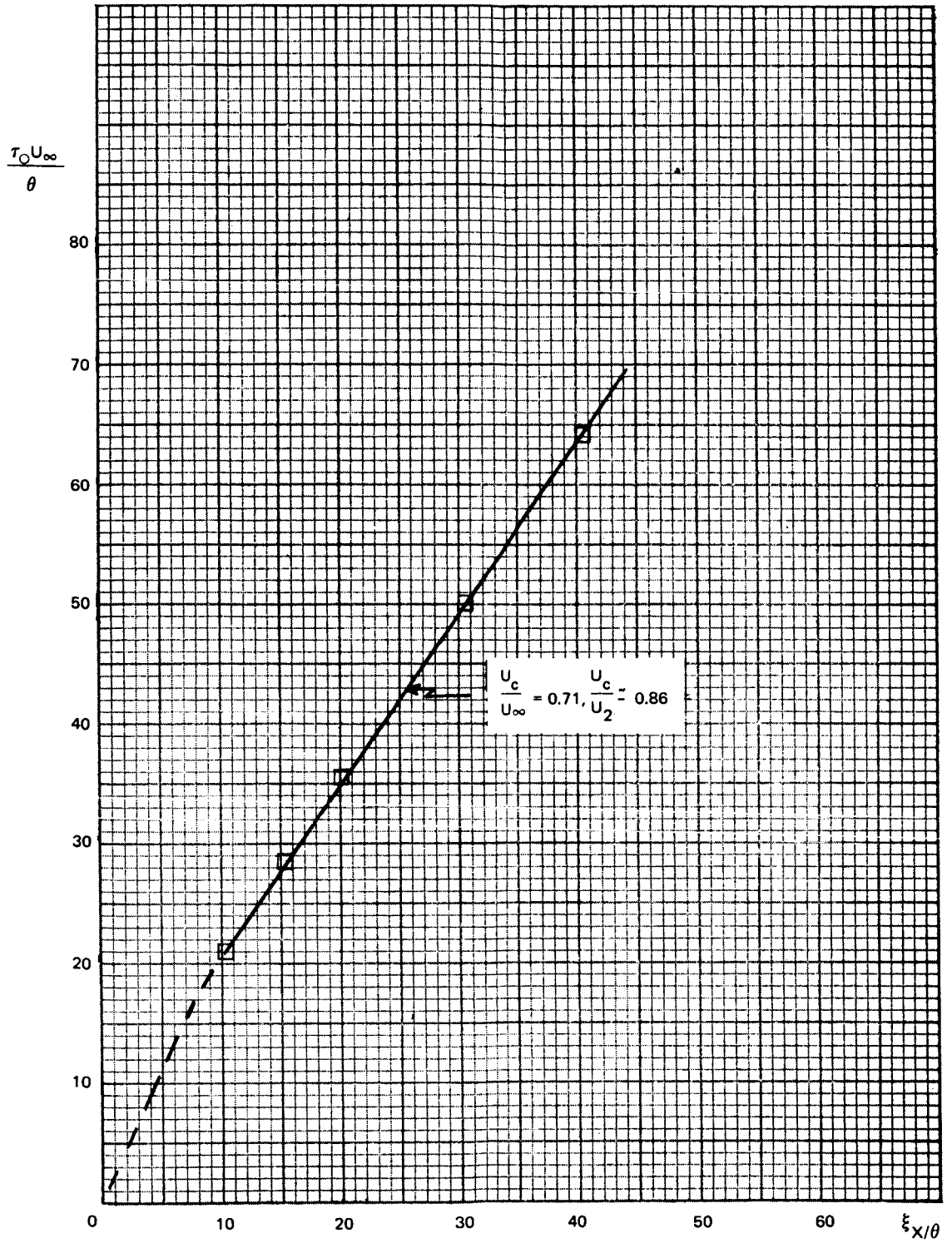

Figure 10. Conjection Time Vs. Spatial Separation in Separated Flow Front of a Forward-Facing Step, M 3.45.

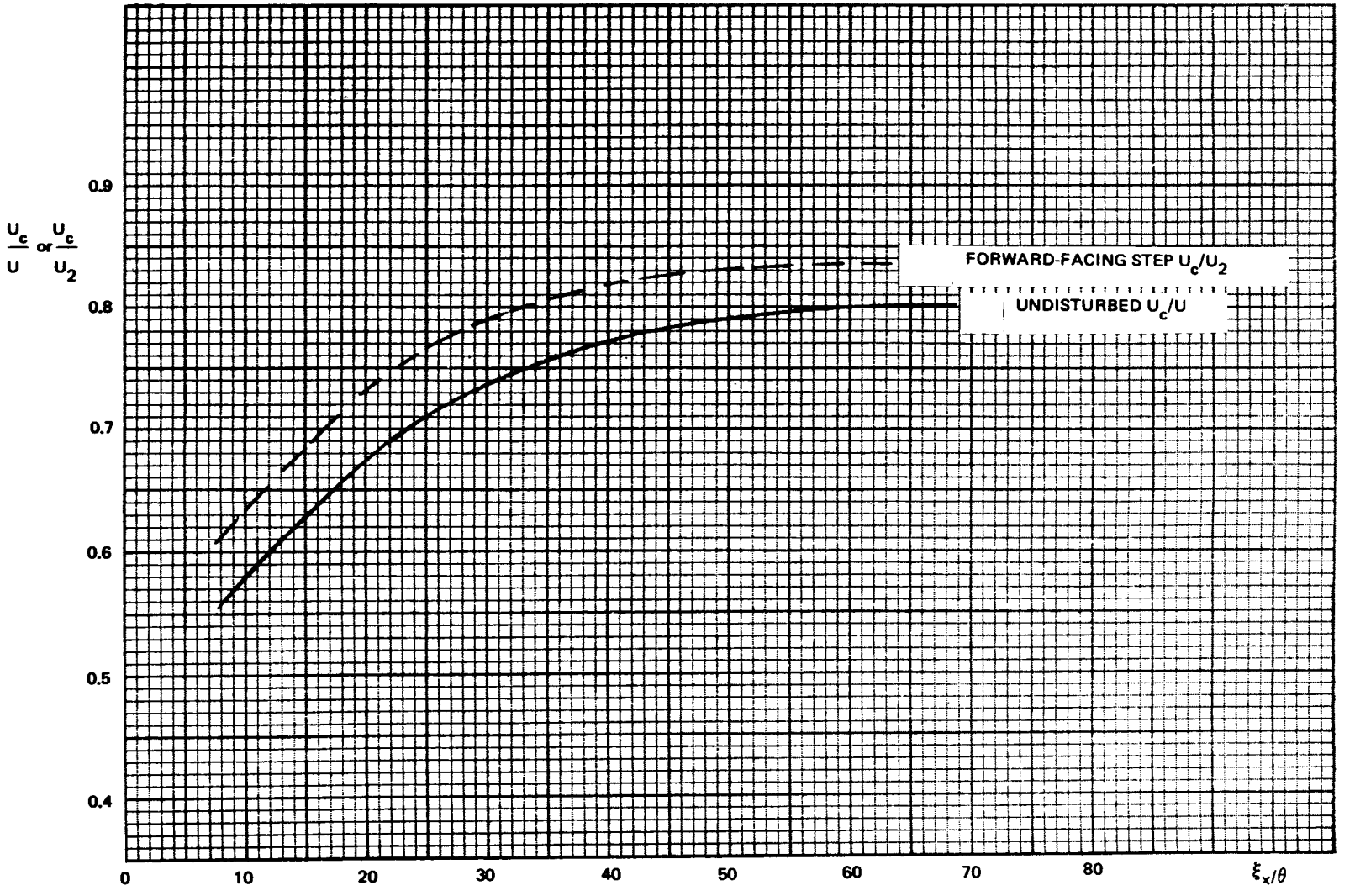

Figure 11. Comparison of Average Convection Velocity for Undisturbed and Forward-Facing Step (In Region of Separated Flow), M 3.45.

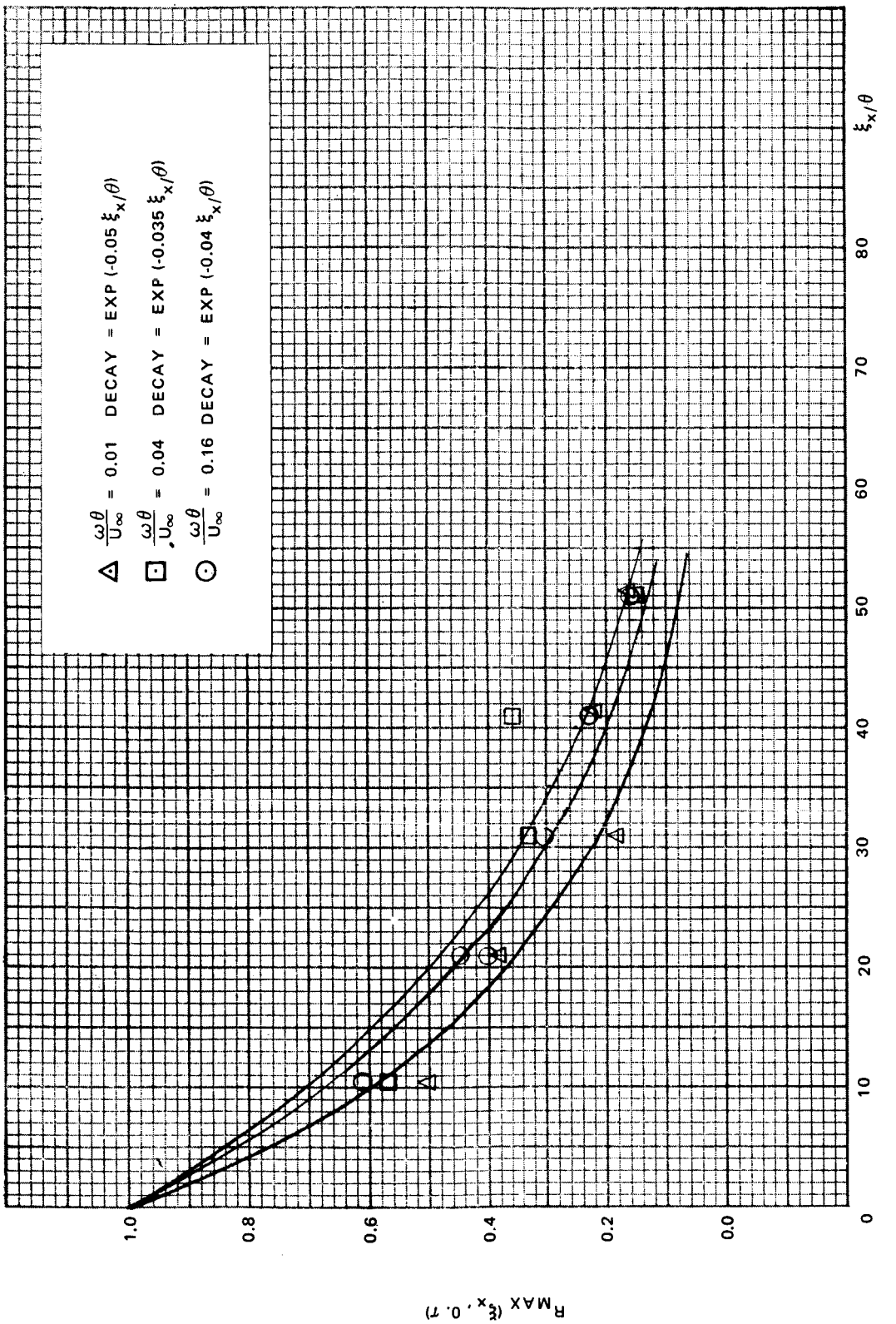

Figure 12. Spatial Decay of Cross-Correlation Maxima for Forward-Facing Step, M 3.45.

Also, frequencies at which these effects occur are usually well beyond the critical first bending mode frequencies of local structure. In addition, the Mach number dependence was not available. The complexity resulting from so many variables negated the usefulness of such a study.

Figure 13 exemplifies this lack of consistency. It shows an average normalized correlation coefficient per incremental area (an area less than one results in normalized correlation coefficients greater than one) versus the nondimensionalized spatial separation distance in the x direction times the center band frequency. When the curve crosses the zero axis, complete pressure cancellation has occurred. However, to be practical as a design chart, the curves for respective L/W (length-to-width ratios) and different narrow bands of data should all collapse onto a single curve. Obviously, this does not happen.

4.4 Shock-Disturbed Flow

In reference 1, difficulty was encountered in analyzing the data from the disturbed flow which was a result of a shock impinging on, and interacting with, the boundary layer. At that time, it was suggested that these data should be examined, using nonstationary data reduction techniques. Some further work has been performed which clarifies certain aspects of the phenomenon.

First, mean squared time histories of several tracks of data (corresponding to locations near the position of shock impingement) were recorded. By inspection, one key position was eliminated as bad or intermittent data. The track in question showed erratic behavior punctuated by voltage spikes of considerable amplitude. This electrical behavior was noted regardless of the physical location of the microphone--whether beneath the shock or well behind it. It was concluded that this track was not operating properly during a portion of the testing period. Unfortunately, the microphone in question was associated with the location directly below the position of shock impingement. Deleting this measurement confined the study to examination of the FPL's in front of the position of impingement, or behind it, but not under or through it. (The spatial extent of the shock impingement was extremely localized).

The recorded data from one microphone, located just in front of the position of shock impingement during a test to investigate FPL characteristics in the direction of the flow and located behind the shock when investigating the direction perpendicular to the flow, indicated the following characteristics: when just in front of the shock, the level of the data increased steadily with time, suggesting that the region of disturbed flow crept slowly upstream during the testing period, but when located behind the position of shock impingement, the data were stabilized at the higher levels indicative of that position. The time-varying data (from in front of the shock) were examined by the technique suggested in reference 7 for time-varying spectra. Mean squared values for frequency-band-limited samples of differing geometrical mean frequencies were time averaged. The resultant mean square for each band of frequencies was then converted to a power-spectrum level by dividing by the respective bandwidths, assuming uniform energy distribution over the band. This calculated power spectrum was then compared to the power

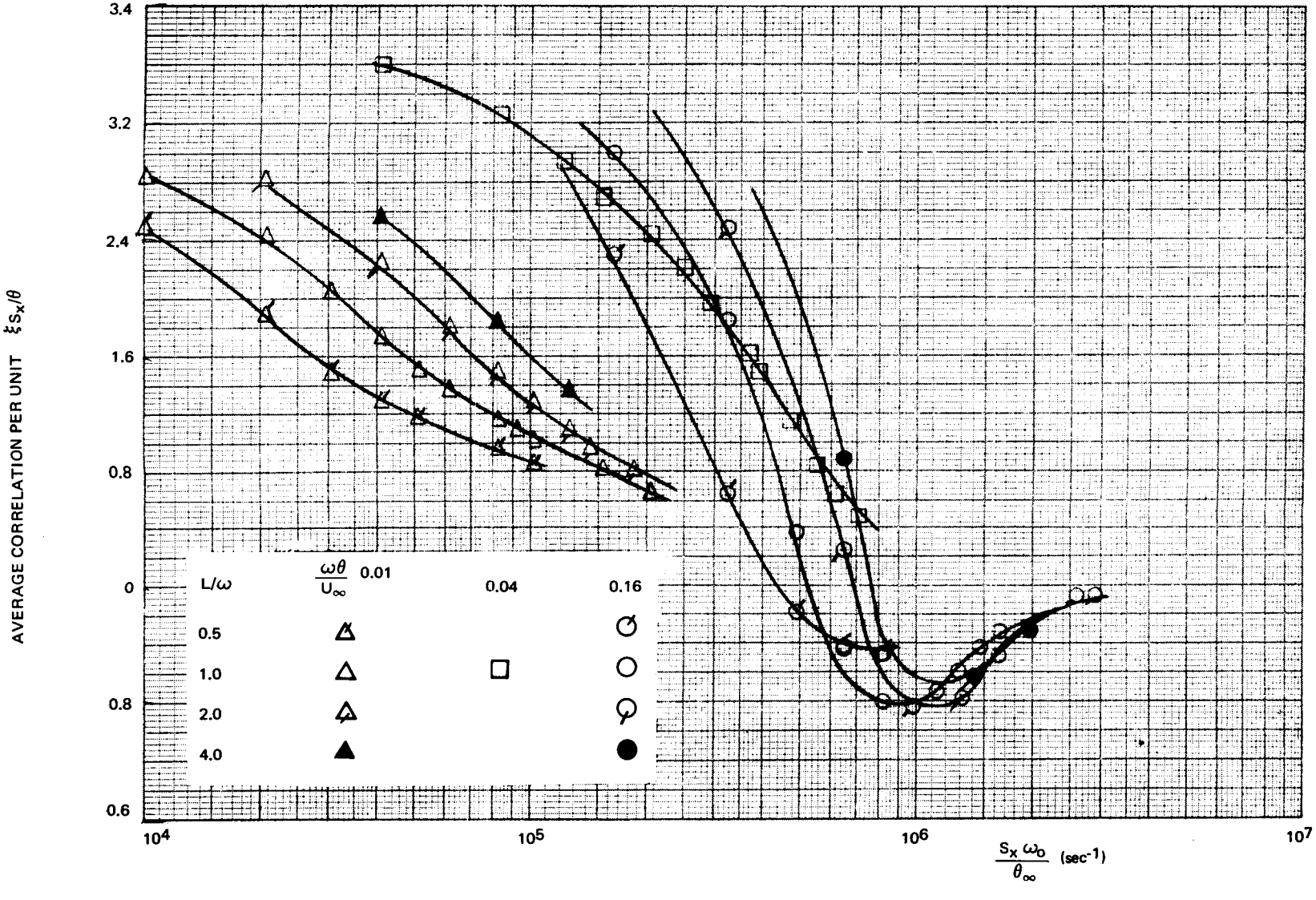

Figure 13. Average Correlation Coefficients Per Incremental Spatial Areas Vs. Frequency and L/W Ratios of Areas.

spectrum originally found when stationarity was assumed, and a small time interval was utilized to calculate an autocorrelation and its Fourier transform, a power-spectral density. The result is plotted in figure 14. The actual magnitudes correlate well for the two positions: prior to and well-behind the position of shock impingement. As can be seen in figure 14, relative changes correlate well, though differences exist between the two methods of data reduction. Since these minor differences are in evidence during both stationary and slowly time-varying or "non-stationary" processes, they can be neglected. Hence, it may be concluded that stationary data processing is permissible on the weakly stationary data involved. As a further check on this conclusion, the two sets of data were examined by means of the test for equivalence of power spectra given in reference 7 (eq. 5.166). The statistical error calculated for each was negligibly small, and the calculation indicated the two pairs of spectra were acceptably the same. This verifies that the weakly stationary data (slowly time-varying signal from in front of the shock) may be as successfully handled by mathematical calculations which assume stationarity as can the data from behind the shock.

No departure from stationarity was in evidence at high frequencies. This is attributable to the time variation being caused by the flow separation moving slowly upstream and the position of interest reflecting the increase in "low"-frequency energy only (indicative of shock-disturbed flow).

All the other data tracks examined exhibited excellent time invariance. With the deletion of the erratic data and substantiation of the data calculations assuming stationarity, the broad band results for shock-disturbed flow were re-examined. As a result, it was established that the convection velocity in the region directly behind the shock-boundary layer interaction was quite low--on the order of $U_c \simeq 0.3U_\infty$ or $U_c \simeq 0.34U_2$ where U_2 was the estimated stream velocity (a function of shock strength) behind the impinging and reflected shocks. It should be noted that unlike other types of flow, no variation in convection velocity was apparent with spatial separation. Also, on the basis of the above evaluation of data validity, it was concluded that the small areas over which the broad band pressure signatures are correlated in the immediate vicinity of a shock wave are correct as quoted in reference 1.

These results might be explained by the following physical interpretation: the impingement of the shock interacts with the boundary layer (sometimes causing flow separation) and generates considerable large-scale (low-frequency) turbulence in the lower strata (low-velocity) region of the boundary layer. These large eddies are quickly dissipated, but the residue of turbulence lasts for a long distance downstream. An estimate can be made of the length (over which residuals are observable) on the basis of static pressure distributions. The estimate for the shock-disturbed flow experiment performed and described in reference 8 was over 10 boundary layer thicknesses downstream.

The narrow band analysis of the shock-disturbed flow data agrees with the above reassessment of the broad band analysis. Figure 15 shows the contours of equal correlation coefficients, while figure 16 indicates the spatial decay for the narrow bands of frequencies examined (again assuming an exponential decay).

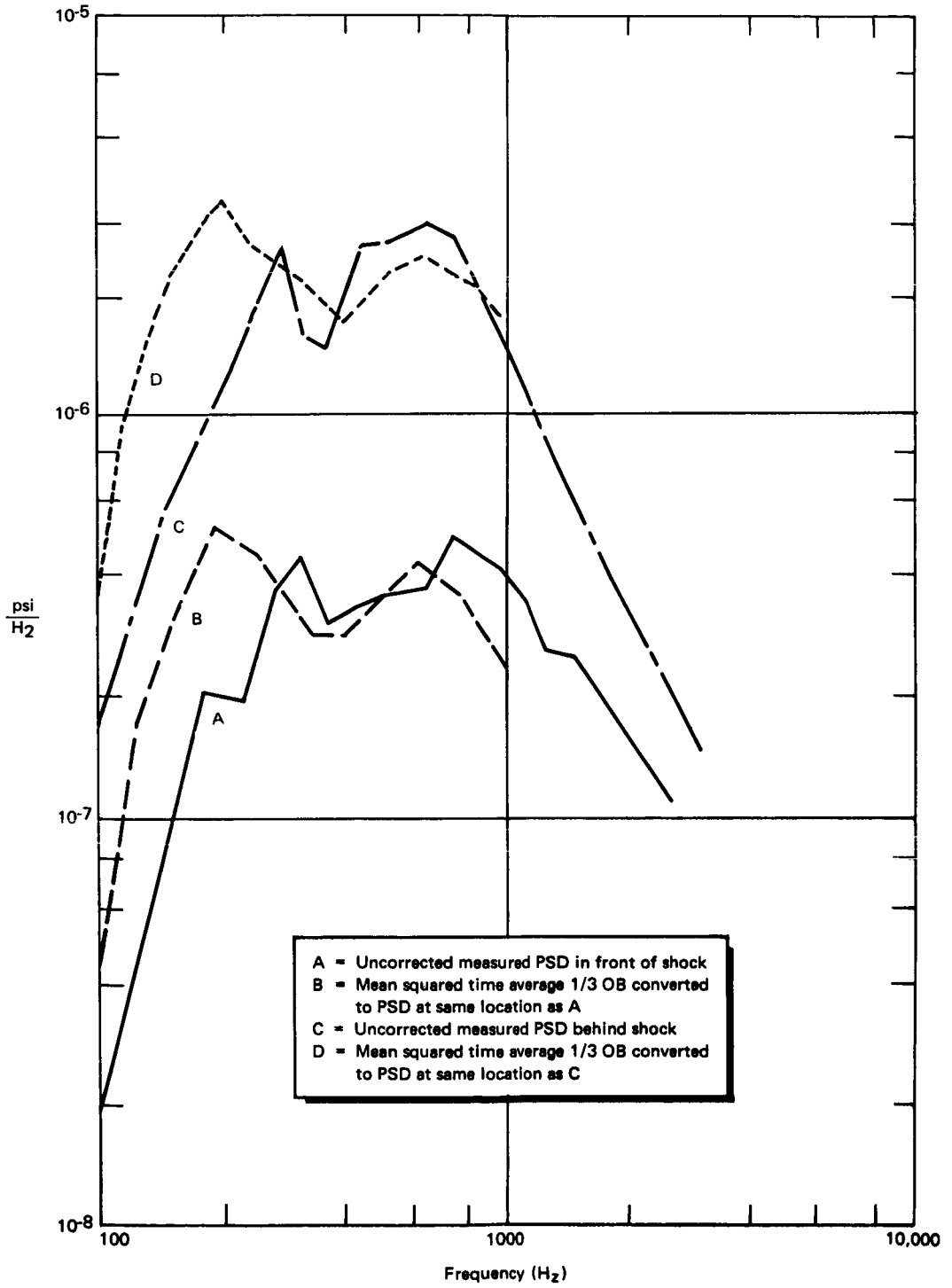

Figure 14. Comparison of PSD's, Assuming Stationarity Vs Time-Averaged Mean Square Determination

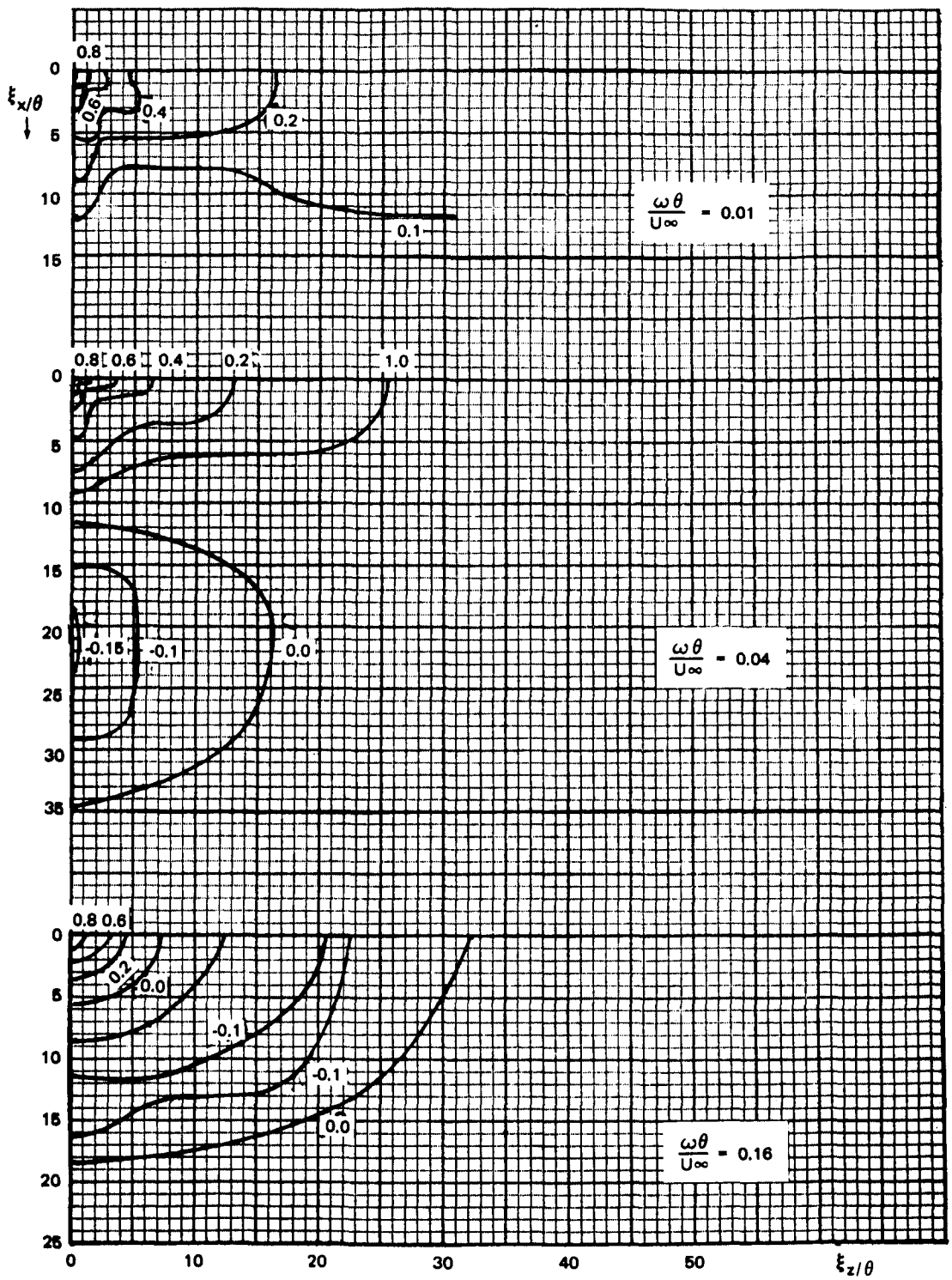

Figure 15. Contours of Equal Correlation Coefficient, Shock – Disturbed Flow, M 3.45.

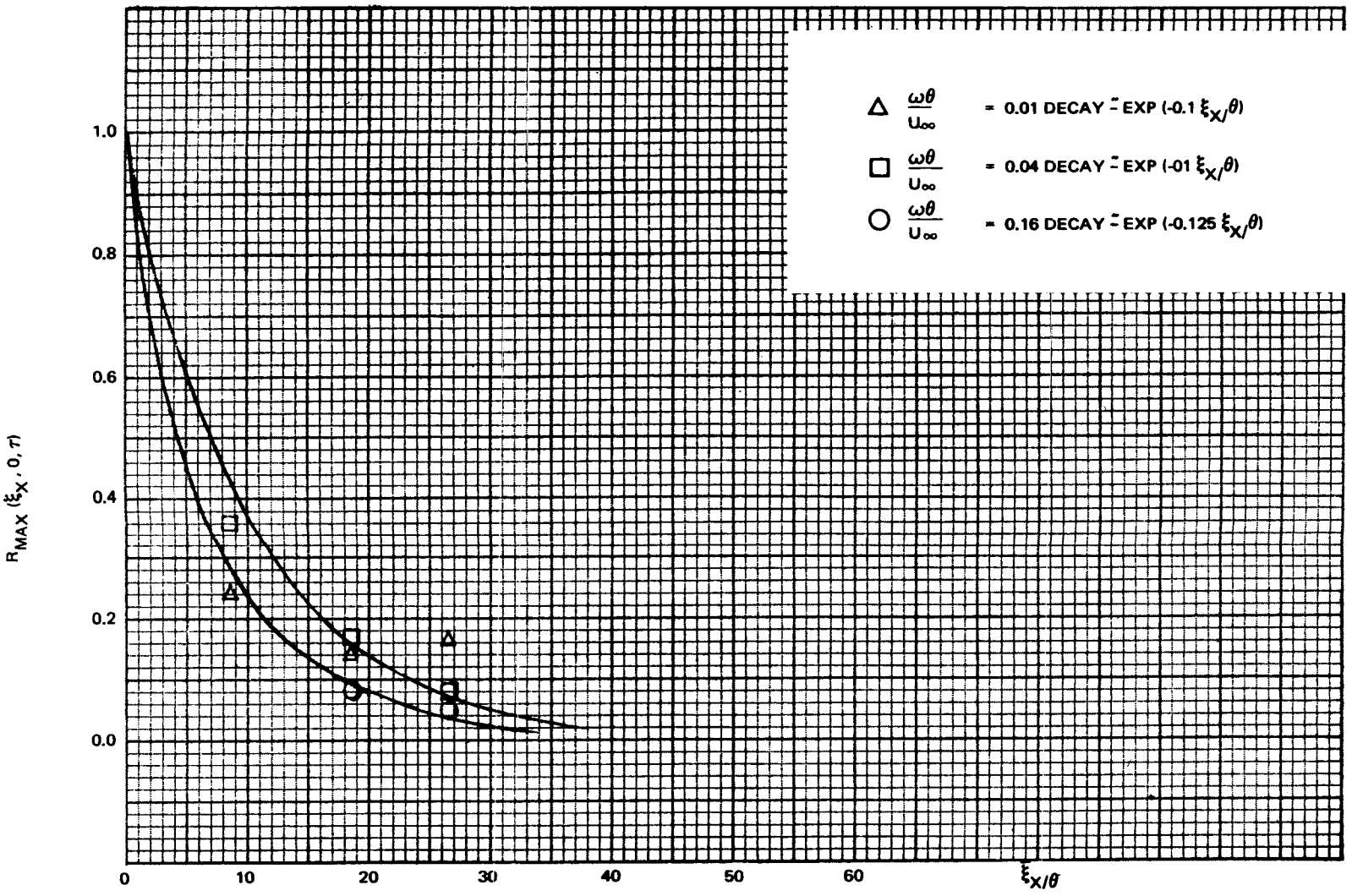

Figure 16. Spatial Decay of the Cross-Correlation Maxima for Shock-Disturbed Flow, M 3.45.

5. DISCUSSION

In this section, transformations are developed by which the variables are separated and mathematical descriptions are found. Influencing factors are discussed, and trends are indicated. Where possible, generalizations have been made which permit comparison of the data with theoretical models of the flow mechanisms that produce the fluctuating pressures at the wall.

5.1 Separability of the Temporal and Spatial Variables

An intuitively appealing and commonly assumed description of broad band cross-correlation functions embodies separability of the temporal and spatial variables in a coordinate system moving with the boundary layer. Since many theoreticians and experimenters have used this assumption in broad band analyses with some success, and several experimenters have used the same assumption for narrow band data, separability in the boundary layer frame was assumed for this analysis. However, results showed some anomalous behavior. This led to a reevaluation of the assumption and its subsequent replacement by an assumption more consistent with the data.

If the assumption of separability in the moving frame is used, data obtained in the fixed frame is transformed to the moving frame by the Galilean transformation pair

$$\begin{aligned} \psi_x &= \xi_x - U_c\tau \\ \psi_t &= \tau \\ \xi_x &= \psi_x + U_c\psi_t \\ \tau &= \psi_t \end{aligned} \qquad (12)$$

where ξ_x, τ are separation distance and time displacement in the fixed frame, U_c is the convection velocity as defined more completely in par. 5.3, and ψ_x, ψ_t are separation distance and time displacement in the moving frame of reference.

Separability in the moving frame can therefore be mathematically expressed as

$$R_x(\xi_x, \tau) = RM(\psi_x, \psi_t) = RM_1(\psi_x)RM_2(\psi_t) = RM_1(\xi_x - U_c\tau)RM_2(\tau) \quad (13)$$

where $R_x(\xi_x, \tau)$ is the cross-correlation in the direction of the flow, RM is the cross-correlation in the moving frame, and RM_1 and RM_2 are the separated spatial and temporal functions. The separated functions may be generated in the following manner. Along the ξ_x axis, $\tau = 0$, and

$$R_x(\xi_x, 0) = RM_1(\xi_x)RM_2(0) = RM_1(\xi_x) \quad (14)$$

Which defines the function RM_1. Projecting the peaks of the cross-correlation, which occurs at $\xi_x = U_c\tau$, on to the τ axis, results in

$$R_x(U_c\tau, \tau) = RM_1(0)RM_2(\tau) = RM_2(\tau) \quad (15)$$

this defines a function RM_2. Both functions are symmetric and have a maximum value of 1, which occurs at the origin. If separability in the moving frame exists, these functions can now be used to predict the cross-correlation at any point in the space-time plane.

In particular, one can predict the autocorrelation and then compare it with the data presented in figure 17. If separability in the moving frame is a valid assumption, the autocorrelation will be (using the symmetry relations presented in paragraph 5.2):

$$R_x(0, \tau) = RM_1(-U_c\tau)RM_2(\tau) = RM_1(U_c\tau)RM_2(\tau) \quad (16)$$

Figures 18, 10, 19, and 20 present the curves $RM_1(\xi_x)$, $\xi_x = U_c\tau$, $RM_2(\tau)$, $RM_1(U_c\tau)RM_2(\tau)$ and the autocorrelation calculated from the data for a forward-facing step at $\omega\theta/U_\infty = 0.16$. The other data have similar behavior. The obvious inconsistency between the autocorrelation predicted by using the assumption of separability in the moving frame and the autocorrelation computed from the data suggests that separability in the moving frame is not a valid assumption for narrow band data.

However, examination of the structure of the mathematical description of a narrow band cross-correlation suggests that there is a frame in which the cross-correlation is separable. Therefore, it is necessary to develop the mathematical description of the cross-correlation.

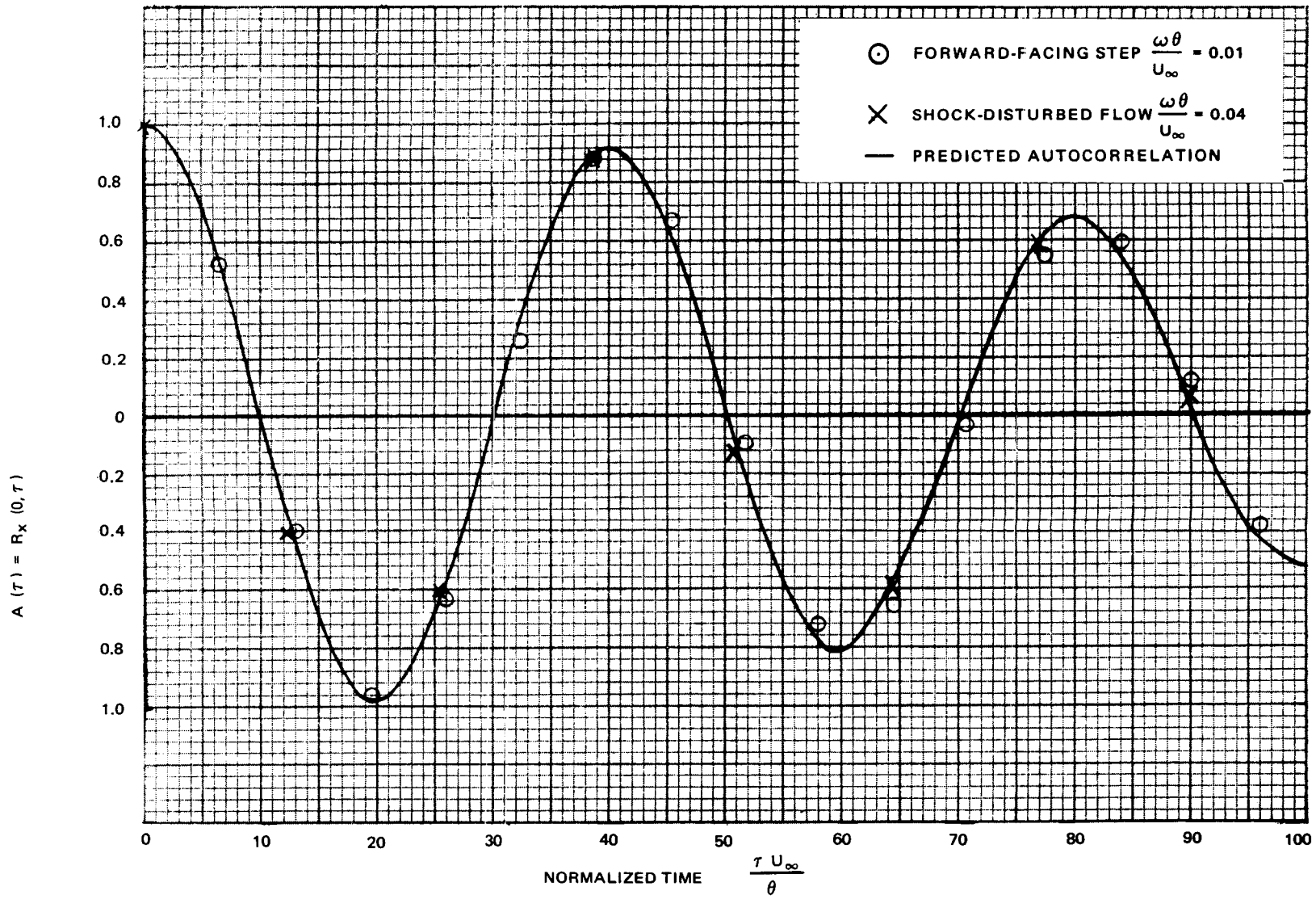

Figure 17. Comparison of Mathematically Predicted and Experimentally Determined Autocorrelation

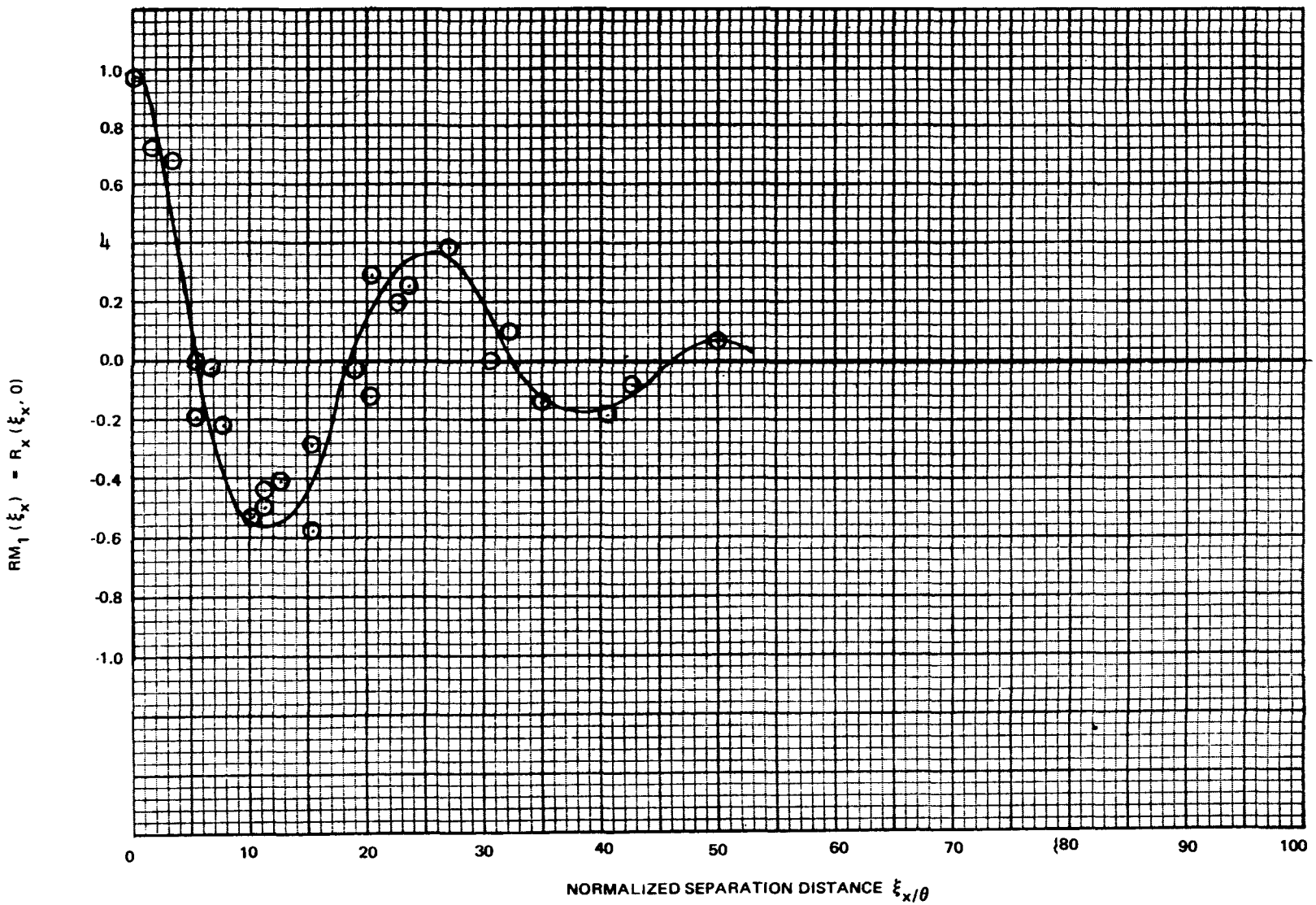

Figure 18. Correlation Coefficient RM_1 (S_X), Forward-Facing Step, M 3.45, $\frac{\omega\theta}{U_\infty}$ = 0.16.

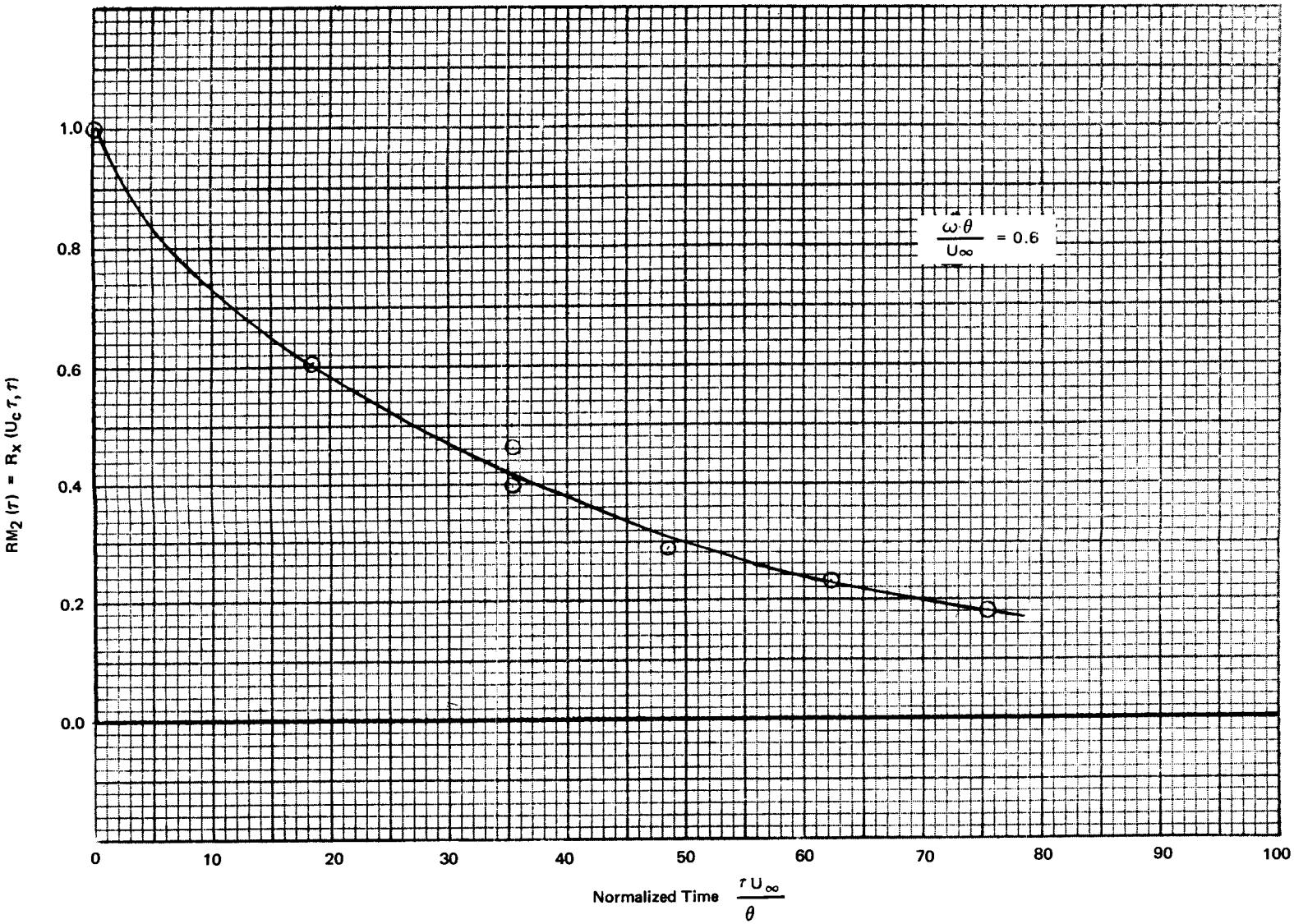

Figure 19. Time Decay in the Moving Frame of Reference, $RM_2(\tau)$, for the Forward-Facing Step, m 3.4.5.

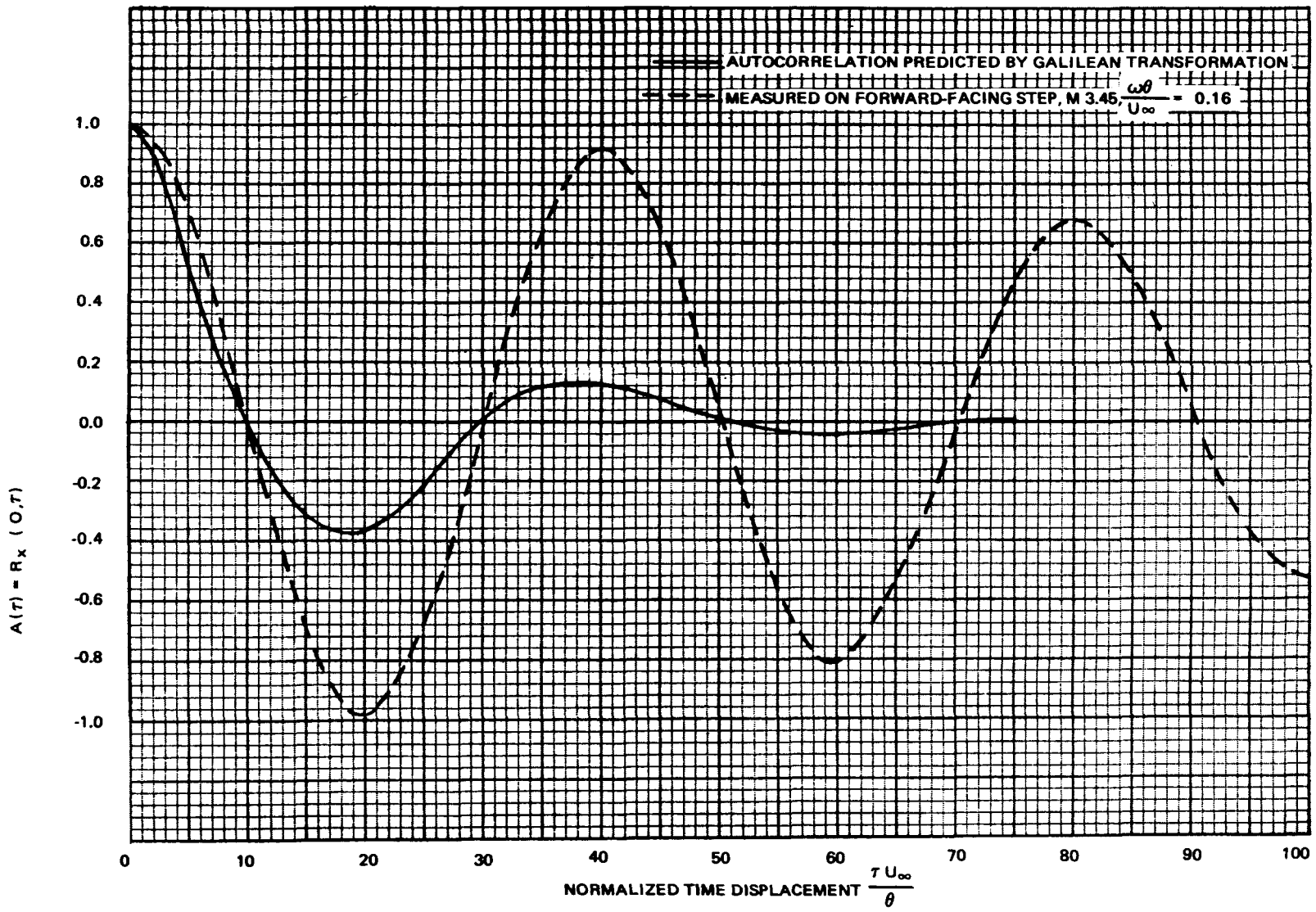

Figure 20. Comparison of Autocorrelation, Predicted by Galilean Transformation, with Experimental Data.

If the bandwidth Δ is sufficiently narrow to approximate the one-sided, cross-spectral density as constant $P_{\alpha\beta}$, and if the flow is nondispersive, the cross-correlation in the fixed frame of reference is

$$R'_x(\tau) = \int_{-\omega_o-\Delta/2}^{-\omega_o+\Delta/2} \frac{P_{\alpha\beta}}{2} e^{-iK\omega} e^{i\omega\tau} d\omega + \int_{+\omega_o-\Delta/2}^{+\omega_o+\Delta/2} \frac{P_{\alpha\beta}}{2} e^{-iK\omega} e^{i\omega\tau} d\omega \tag{17}$$

$$= \int_{\omega_o-\Delta/2}^{\omega_o+\Delta/2} P_{\alpha\beta} \cos\{\omega(\tau - K)\} d\omega = P_{\alpha\beta} \frac{\sin\{\omega(\tau - K)\}}{(\tau - K)} \Bigg|_{\omega_o-\Delta/2}^{\omega_o+\Delta/2}$$

normalizing by $1/\Delta\sqrt{P_\alpha P_\beta}$

$$R_x(\tau) = \frac{P_{\alpha\beta}}{\sqrt{P_\alpha P_\beta}} \frac{\sin\{\Delta/2(\tau - K)\}}{\{\Delta/2(\tau - K)\}} \cos\{\omega_o(\tau - K)\} \tag{18}$$

where K is the rate of change of phase-angle with frequency. If a non-zero slope of the cross-spectrum is taken into account, the effect is of order $(\tau - K)^2$ and, therefore, does not strongly influence the results near the peak $(\tau = K)$. The effect of non-zero slope was found to be less than 5% for all flows and frequency ranges, for the times considered in this study

$$\left(\frac{\tau U_\infty}{\theta} \leq \frac{5\pi}{\frac{\omega\theta}{U_\infty}}\right)$$

Similarly, small amounts of dispersion do not seriously effect the results.

Figure 20 indicates the predicted autocorrelation which is identical to the cross-correlation evaluated for K = 0, and compares it with representative experimental autocorrelation points. When the pressure is acting on a structure with low damping, the structure responds only to the Fourier components of the pressure in a band of frequencies near the resonance frequencies of the structure. Hence, the structure acts like a filter on the pressure signature. The bandwidth of the filter corresponds to the width of the resonance peak of the structure, and the center frequency of the filter corresponds to the resonance frequency itself. The width of the resonance peak is usually measured in terms of Q, the dynamic amplification factor,

$$\Delta = \frac{\omega_o}{Q} \tag{19}$$

The general form of the normalized narrow band cross-correlation in terms of the structural variable Q and resonance frequency ω_o is

$$R_x(\tau) = \frac{P_{a\beta}}{\sqrt{P_a P_\beta}} \frac{\sin\left|\frac{\omega_o}{2Q}(\tau - K)\right|}{\left|\frac{\omega_o}{2Q}(\tau - K)\right|} \cos\{\omega_o(\tau - K)\} \tag{20}$$

The data indicated that for most frequency ranges and most flows the narrow band data could be represented as having a constant amplitude cross-spectrum within the band and as being nondispersive. Hence, for sufficiently narrow bands ($\Delta \leq \omega_o/4$), the cross-correlations will be identical except for an amplitude factor and translation of the peak to $\tau = K$. The rate of change of phase angle with frequency, K, is equal to the ratio of separation distance to convection velocity, $\xi_x = U_c K$. Since the amplitude of the cross-spectrum $P_{a\beta}$ is, in general, only a function of separation distance, the narrow band cross-correlation can be written

$$R_x(\xi_x, \tau) = \frac{P_{a\beta}(\xi_x)}{\sqrt{P_a P_\beta}} \frac{\sin\left|\frac{\omega_o}{2Q}\left(\tau - \frac{\xi_x}{U_c}\right)\right|}{\left|\frac{\omega_o}{2Q}\left(\tau - \frac{\xi_x}{U_c}\right)\right|} \cos\left|\omega_o\left(\tau - \frac{\xi_x}{U_c}\right)\right| \tag{21}$$

This is of the form

$$R_x(\xi_x, \tau) = RT_1(\xi_x) RT_2\left(\tau - \frac{\xi_x}{U_c}\right) \tag{22}$$

This means that the cross-correlation is separable using the transform pair

$$\begin{aligned} \eta_x &= \xi_x \\ \eta_\tau &= \tau - \frac{\xi_x}{U_c} \\ \xi_x &= \eta_x \\ \tau &= \frac{\eta_x}{U_c} + \eta_\tau \end{aligned} \tag{23}$$

where η_x and η_τ are the spatial and temporal coordinates in a retarded time frame of reference. So the cross-correlation may be written

$$R_x(\xi_x,\tau) = RT(\eta_x,\eta_\tau) = RT_1(\eta_x)RT_2(\eta_\tau) = RT_1(\xi_x)RT_2\left(\tau - \frac{\xi_x}{U_c}\right) \qquad (24)$$

where RT is the cross-correlation in the retarded time frame, and RT_1 and RT_2 are the separated spatial and temporal functions. The separated functions may be generated in the following manner: along $\xi_x = 0$, the autocorrelation,

$$R_x(0,\tau) = RT_1(0)RT_2(\tau) = RT_2(\tau) \qquad (25)$$

which generates the function RT_2. If the peaks of the cross-correlation, which occur at $\xi_x = U_c\tau$, are projected on the ξ_x axis

$$R_x\left(\xi_x,\frac{\xi_x}{U_c}\right) = RT_1(\xi_x)RT_2(0) = RT_1(\xi_x) \qquad (26)$$

which generates the function RT_1.

If separability in the retarded time frame exists, the separated functions should be able to predict the cross-correlation at any point in the space-time plane. In particular, the spatial correlation $R_x(\xi_x, 0)$ can be predicted and compared with the experimental data. If the assumption of separability in the retarded time frame is correct, the spatial correlation will be (using the symmetry relation in par. 5.2):

$$R_x(\xi_x, 0) = RT_1(\xi_x)RT_2\left(-\frac{\xi_x}{U_c}\right) = RT_1(\xi_x)RT_2\left(\frac{\xi_x}{U_c}\right) \qquad (27)$$

The appropriate curves are given for $RT_1(\xi_x)$ (fig. 12); $\xi_x = U_c\tau$ (fig. 10); $RT_2(\tau)$ (fig. 17); $RT_1(\xi_x)RT_2(\xi_x/U_c)$ and the spatial correlation from the experimental data are presented in figure 21. The good agreement between predicted and experimental spatial correlation provides strong support for the assumption of separability in the retarded time frame of reference.

5.2 Implications of a Retarded Time Transformation

The use of a retarded time frame instead of a frame moving with the boundary layer has many implications. In this section, a mathematical interpretation of the effect of the two transformations on the separation distance-time correlation space is presented.

Figure 21. Comparison of Spatial Correlation $RT_1(\xi_x)$ RT_2 $\frac{\xi x}{U_\infty}$ Predicted by Retarded Time Transformation with Data

The effects of the two coordinate transformations discussed in paragraph 5.1 can be more easily visualized in terms of a three-dimensional surface in correlation-separation distance-time displacement space. Figures 22 through 24 represent the surface for the fixed frame, the frame moving with the boundary layer, and the retarded time frame. The coordinate transformations act on the space-time plane. Their effect can be more easily understood by considering the shaded rectangle in the fixed plane (fig. 2).

The effect of the Galilean transformation from the fixed frame to the moving frame,

$$\psi_x = \xi_x - U_c\tau$$
$$\psi_\tau = \tau \qquad (28)$$

is to shear the plane in the negative direction parallel to the spatial axis by an amount $U_c\tau$. For purposes of illustration, U_c has been drawn as constant, which is not generally true. The rectangle becomes a parallelogram and the diagonal of the rectangle ($\xi_x = U_c\tau$) is mapped into the diagonal of the parallogram which coincides with the temporal axis. The effect of the retarded time transformation,

$$\eta_x = \xi_x$$
$$\eta_\tau = \tau - \frac{\xi_x}{U_c} \qquad (29)$$

is similar to that of the Galilean transformation. In this case, however, the shearing is parallel to the temporal axis by the amount ξ_x/U_c, and the diagonal of the parallelogram ($\xi_x = U_c\tau$) coincides with the spatial axis.

The effect of the transformations on the cross-correlation can be more easily understood in terms of amplitude and phase lines. An amplitude line is a line along which the envelope of the cross-correlation has constant amplitude except for bandwidth attenuation. It is a line along which the envelope would have constant amplitude for an infinitely narrow filter. In particular, recalling the mathematical description of a narrow band cross-correlation (eq. 21), it is a line where $P_{\alpha\beta}$ is constant, a line of constant ξ_x.

Similarly, a line of constant phase is one along which the phase of the cosine function is constant. Since the line $\xi_x = U_c$ is determined as the location of peaks of the cross-correlation, it is a line of constant phase. As shown in figures 22 to 24, the Galilean transformation brings the lines of

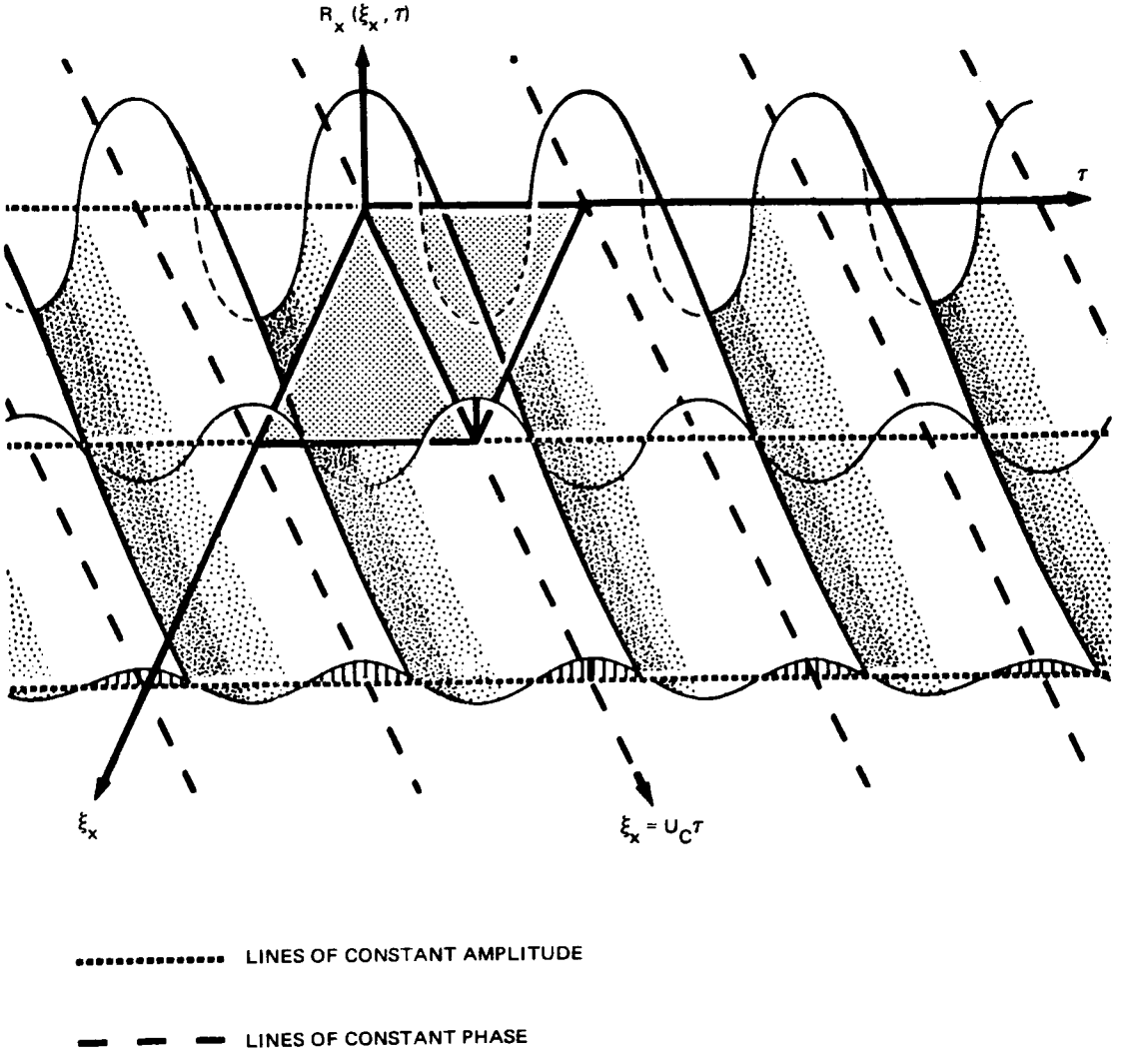

Figure 22. Cross-Correlation in the Fixed Frame of Reference

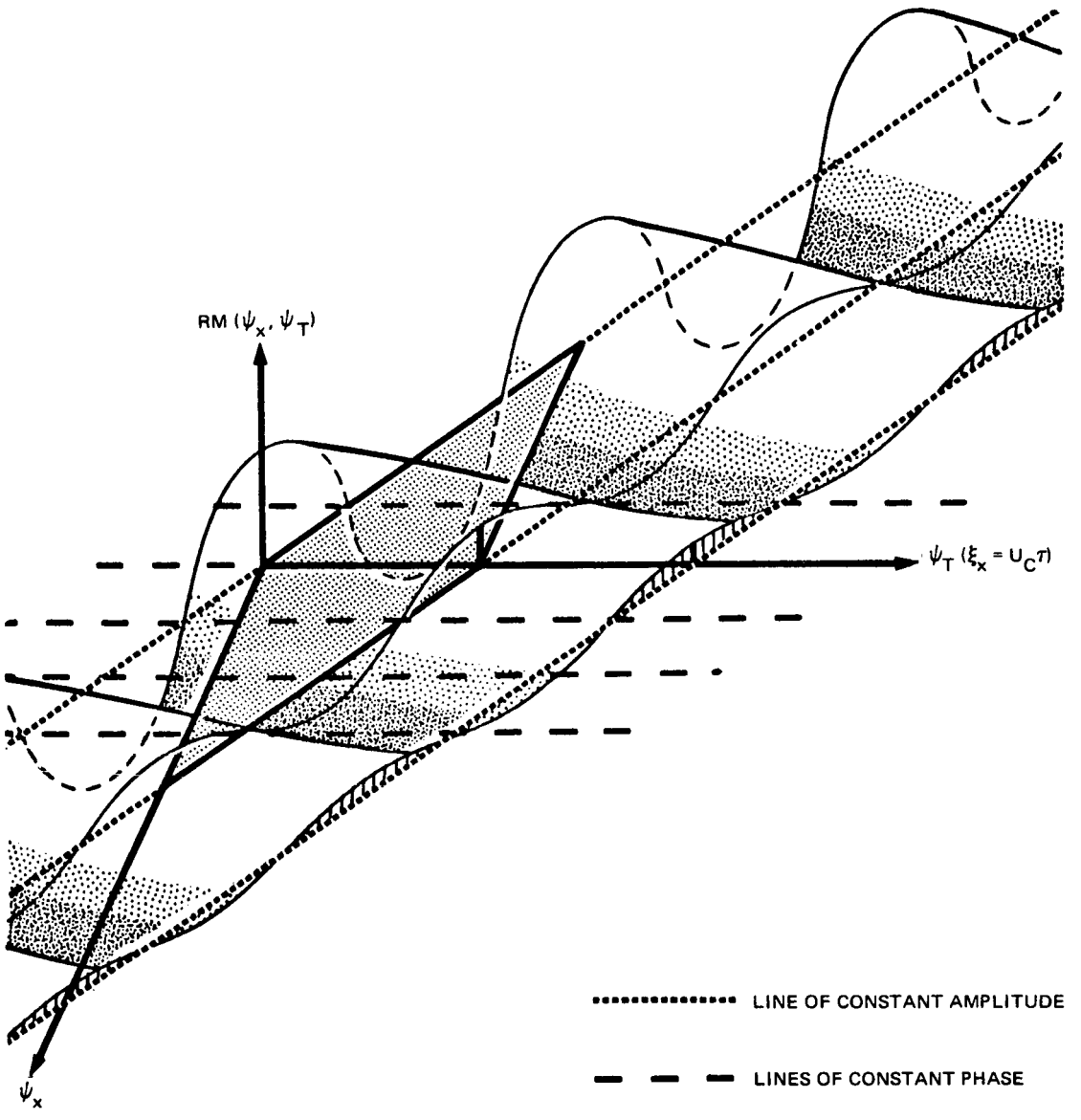

Figure 23. Cross-Correlation in the Moving Frame of Reference

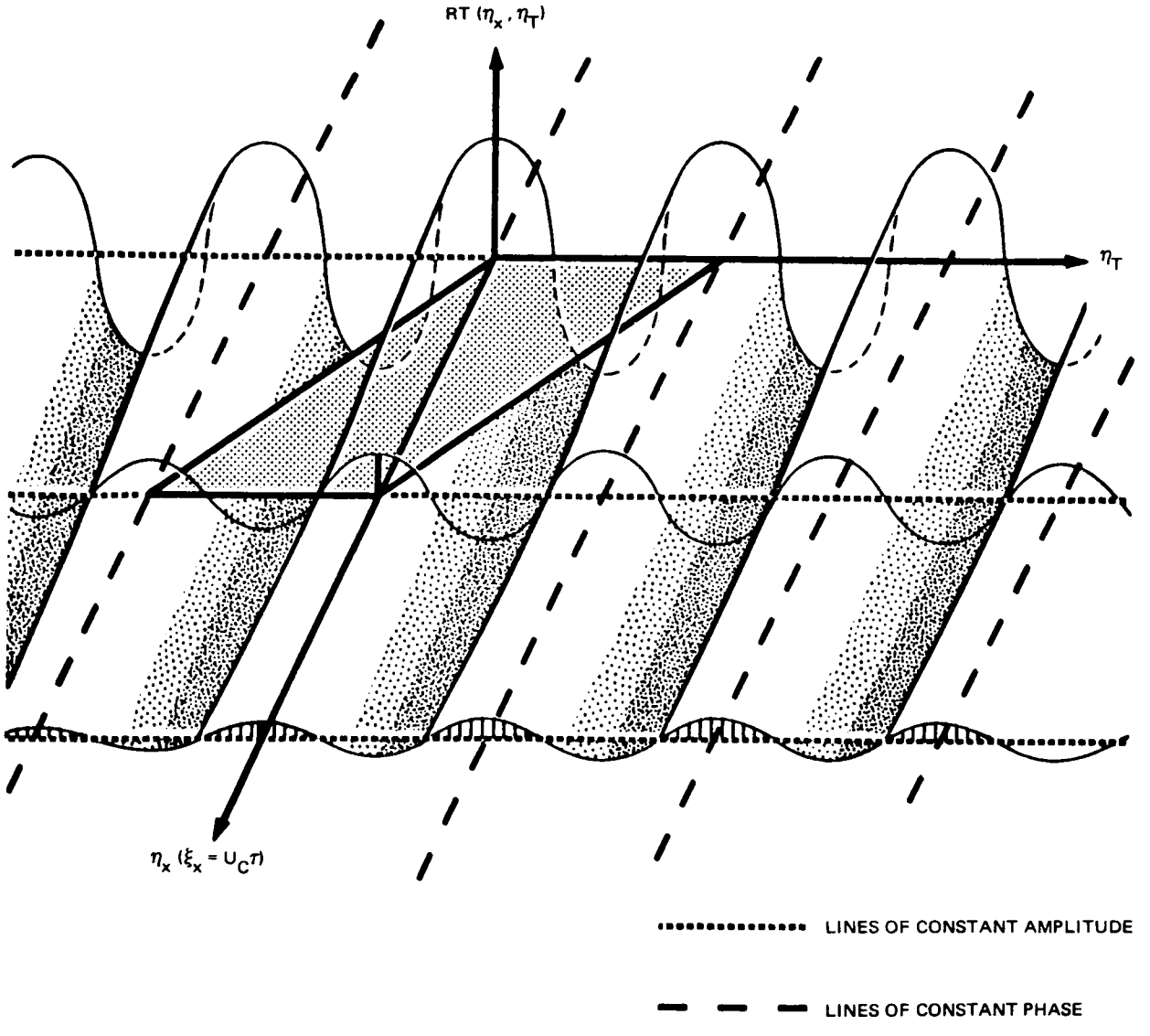

Figure 24. Cross-Correlation in the Retarded Time Frame of Reference

constant phase parallel to the temporal axis, but the lines of constant amplitude are now parallel to the line $\psi_x = -U_c\psi_t$. However, the retarded time transformation does not affect the amplitude lines, but the phase lines are brought parallel to the spatial axis. It can be seen that only in the retarded time coordinate system are the phase and amplitude lines orthogonal. Therefore, it is only in the retarded time system that the cross-correlation can be described as a product of an amplitude curve and a phase curve.

The basic symmetry properties of the cross-correlation provide some insight into the two transformations and provide additional support for the retarded time transformation. The basic symmetry stems from the fact that reversing microphones and then reversing the time displacement cannot affect the cross-correlation, so in the fixed frame, the cross-correlation has a center of symmetry at the origin,

$$R_x(-\xi_x, -\tau) = R_x(\xi_x, \tau) \tag{30}$$

Both of the coordinate transformations are symmetric so the same symmetry relations hold in the transformed coordinate systems. This implies the separated functions RM_1, RM_2, RT_1, RT_2 must also be symmetric. If these functions are symmetric, it follows that in any coordinate system where separability is to hold, the coordinate axes must be lines of symmetry. In other words,

$$R(\xi_x, \tau) = R(-\xi_x, \tau) = R(-\xi_x, \tau) = R(\xi_x, -\tau) \tag{31}$$

it was shown in paragraph 5.1 that the cross-correlation is symmetric about $\tau = K$ ($\xi_x = U_c\tau$). For any fixed separation then, referring to figure 23, it is clear that symmetry about the coordinate axes is violated in the frame moving with the boundary layer. However, in the retarded time frame (fig. 24) the symmetry requirements are met.

It has been shown that the retarded time frame of reference agrees well not only with what is mathematically expected but also with experimental data. This is in contradiction to the assumption of separability in the frame moving with the boundary layer which has been successfully used for broad band work. Therefore, one of the following three conclusions must be reached: (1) the data taken in this experiment are not representative of true narrow band phenomena; (2) there is no contradiction because narrow band and broad band phenomena do not behave in the same manner; or (3) the assumption of separability in the moving frame is not correct for the broad band. Further research will be required to absolutely determine which of these conclusions is correct; however, some of the arguments for each are presented at this time.

The first hypothesis is that the method of data analysis used in this experiment does not completely and accurately extract narrow band information. That is, if the sources of pressure fluctuation were acting in only a certain band of frequencies, their cross-correlations would not be the same

as the cross-correlations produced by filtering tape-recorded pressure fluctuations that were caused by sources with a wide range of frequencies. If the pressure time history at a given transducer has a narrow band power spectral density, then the cross-spectral density must have the same narrow band, because by definition (eq. 1) it is the expected value of the product of the signals, both filtered at the same frequency; and because the signal from the first transducer, filtered at any frequency outside its band, is zero. This means that no cross-correlation information could be lost by filtering the cross-spectral density. It can be mathematically shown (ref. 9) that the cross-correlation associated with filtering the cross-spectral density is identical to the cross-correlation associated with filtering each channel with identical filters--the method of data reduction used in this experiment. This suggests that no cross-correlation information was lost, and, therefore, suggests that this experiment did extract the narrow band information completely and accurately.

The second hypothesis is that the broad band data and narrow band data are related in a complex manner. The general form of the narrow band cross-correlation is

$$R'_x(\xi_x, \tau, \omega_o, \Delta) = \Delta P_{\alpha\beta}(\xi_x, \omega) \frac{\sin \frac{\Delta}{2}\left(\tau - \frac{\xi_x}{U_c}\right)}{\frac{\Delta}{2}\left(\tau - \frac{\xi_x}{U_c}\right)} \cos \omega_o\left(\tau - \frac{\xi_x}{U_c}\right) \tag{32}$$

In the limit, as the bandwidth tends to zero, this becomes the differential:

$$d\, R'_x(\xi_x, \tau, \omega) = P_{\alpha\beta}(\xi_x, \omega) \cos \omega\left(\tau - \frac{\xi_x}{U_c}\right) d\omega \tag{33}$$

so the broad band cross-correlation is

$$R'_x(\xi_x, \tau) = \int_0^\infty P_{\alpha\beta}(\xi_x, \omega) \cos \omega\left(\tau - \frac{\xi_x}{U_c}\right) d\omega \tag{34}$$

as would be expected.

Now, since

$$\gamma^2_{\alpha\beta}(\xi_x, \omega) = \frac{\left[P_{\alpha\beta}(\xi_x, \omega)\right]^2}{P_\alpha(\xi_x, \omega) P_\beta(\xi_x, \omega)} \tag{35}$$

and assuming homogeneous data

$$P(\omega) = P_{\alpha}(\xi_x, \omega) = P_{\beta}(\xi_x, \omega) \tag{36}$$

the broad band cross correlation is

$$R'_x(\xi_x, \tau) = \int_0^{\infty} P(\omega) \sqrt{\gamma^2_{\alpha\beta}(\xi_x, \omega)} \cos \omega\left(\tau - \frac{\xi_x}{U_c}\right) d\omega \tag{37}$$

This is not in general separable. If, however, the coherence is not a function of frequency or is only weakly frequency-dependent, this may be approximated by

$$R'_x(\xi_x, \tau) = \sqrt{\gamma^2_{\alpha\beta}(\xi_x)} \int_0^{\infty} P(\omega) \cos \omega\left(\tau - \frac{\xi_x}{U_c}\right) d\omega \tag{38}$$

which is separable in the time retarded frame. This suggests that the broad band data are not, in general, separable, and that in those cases where it is separable, the retarded time frame may be of most value.

The third hypothesis is that the retarded time frame is the most useful, and should be used for both broad band and narrow band data. Typically, broad band cross-correlations are a single peak whose width in time displacement is small compared to the time decay curve. The anomalous behavior presented in paragraph 5.1 is most noticeable far from the peak of the correlation, thus the difference in the two methods is small for broad band data. In the limit of infinitely broad band white noise, the cross-correlation becomes a delta function, and the two methods are exactly equivalent. This means that presenting broad band data using a Galilean transformation might be less useful, but the magnitude of the error introduced would be small. This also suggests that the broad band data could be presented in the retarded time frame at least as well as in the method it has been presented in previously.

Correlation measurements alone cannot be used to describe the physical nature of the flow. However, the behavior of the correlation does provide some insight into the nature of the flow. The retarded time coordinate transformation corresponds to starting a downstream record later than the upstream record by an amount equal to the time taken for the signal to be convected to the downstream location, since for narrow band data, the amount of decay depends primarily on separation distance. One explanation for this decay mechanism is the presence of an incoherent source along the wall being constantly introduced over all space rather than a mechanism such as eddy decay. Convection velocity studies seem to substantiate this

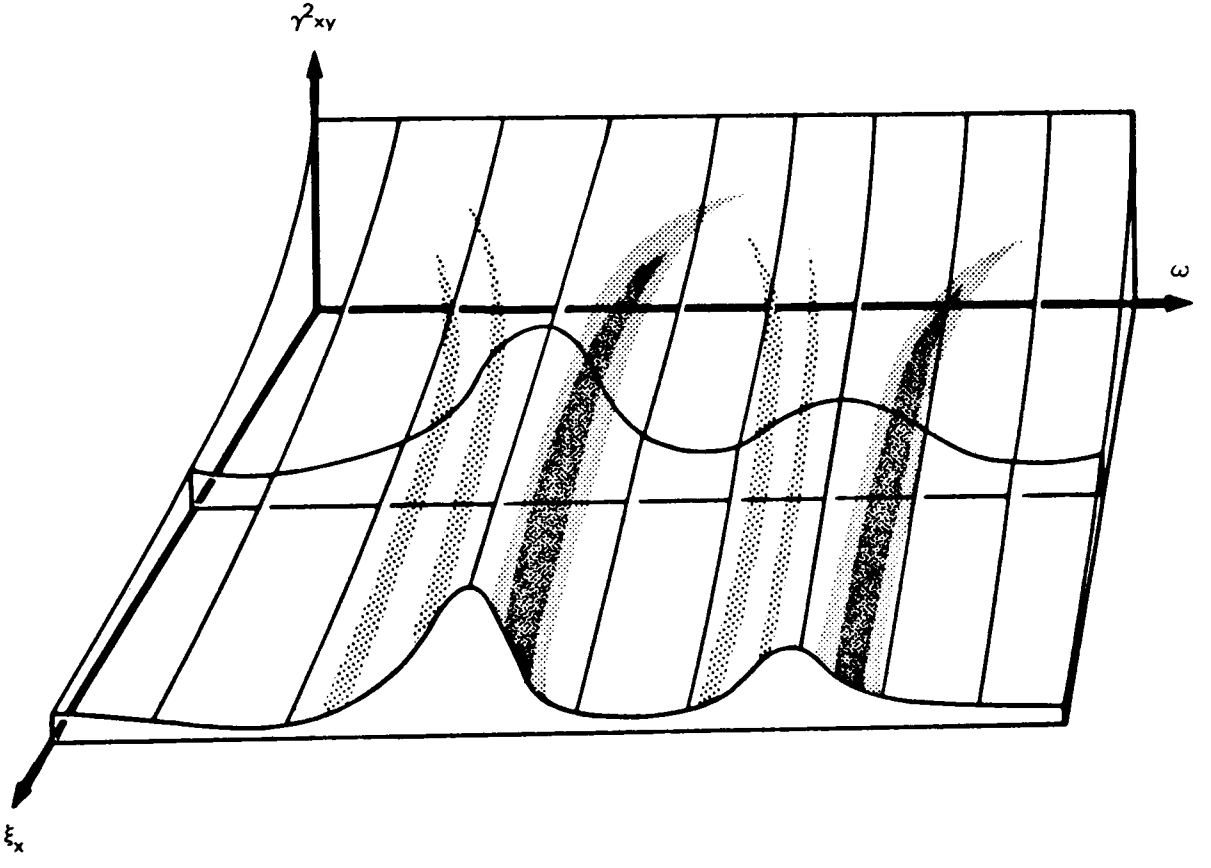

Figure 25. Typical Coherence Surface in Frequency-Separation Distance Space

proposition. However, a completely accurate description of the decay mechanism must be a topic for further research.

5.3 Discussion of the Coherence Function

The coherence function (γ^2_{xy}) is defined as the ratio of the magnitude of the cross-spectral density squared to the product of the power spectral densities of the two signals. Hence, the coherence function is the square of the peak amplitude of the normalized narrow band cross-correlation. The coherence function will therefore have the same resolution bandwidth as the resolution of the power spectral density (see par. 3.5.3). It presents spatial decay information. At any frequency ω_o, a plot of the square root of coherence function with separation distance corresponds to the peaks of the cross-correlation projected on the separation axis. This corresponds to the separated spatial decay curve $RT_1(\xi_x)$ (see para. 5.1). Although the coherence function presents the decay information unencumbered by phase information, it is subject to statistical scatter even greater than that of the power spectral density (because it is proportional to the square of the cross-spectral density). This means detailed decay curves cannot be obtained from the coherence function with the statistical error usually found in broad band analysis. However, they can be used to indicate general trends with respect to frequency. In the limit, as separation distance approaches zero, the cross-spectral density is identical to the power spectral densities of the individual signals, so the coherence function is unity for all frequencies.

For undisturbed flow, the coherence function for non-zero separation appears as a broad resonance at $\omega\theta/U_\infty \approx 0.08$, rolling off slightly at lower and higher frequencies. As the separation distance becomes small, the peak seems to shift to higher frequencies. However, since for small separation distances the coherence function tends to unity for all frequencies, the definition of the peak is reduced. In addition, the statistical scatter masks the peak, making it difficult to accurately measure the frequency at which the peak occurs.

The coherence function for aft- and forward-facing steps exhibit, in many cases, several sharp well-defined peaks. Figure 25 illustrates the behavior for a forward-facing step near the step. In this case there are two peaks occurring at $\omega\theta/U_\infty \approx 0.10$ and $\omega\theta/U_\infty \approx 0.16$. Such peaks seem to occur at the same frequency for all separations in a particular region of a particular flow. However, the patterns change significantly with distance from the step face, and the type of flow examined. In general, frequencies of the peaks are low near the step face and increase when the region of separation or reattachment is approached. In the vicinity of separation or reattachment the behavior is markedly different. The sharp peaks in the coherence function suggest the existance of a resonance type of phenomenon associated with the region inside the separated flow. Since the peaks seem to rise in frequency as the flow nears the wall, it might be hypothesized that the resonance is associated with the height of the cavity inside the separated flow rather than with the volume.

The coherence function for the shock-disturbed flow has a significant peak only at very low frequency. As indicated in reference 1, the energy seems to be concentrated in the low frequencies. This suggests that a

low-frequency phenomenon is associated with shock-disturbed flow (see par. 4.4). To define this phenomenon more exactly would require longer record lengths than are usually possible due to data nonstationarity. Some of the difficulties associated with low frequency and long record length data reduction are discussed in paragraph 3.5.3.

The presence of resonance-type peaks in most types of flow illustrate why it is not possible to interpolate between the decay curves presented in section 4. If the two frequencies reported fell on either side of a peak, an interpolated decay curve for a frequency near a resonance peak would be grossly non-conservative in estimating the area over which the flow is correlated. The data indicates that peaks do exist between frequencies for which decay curves were plotted so the decay curves cannot be used for interpolation. Further study of these effects would be required to provide more detailed information on the frequency dependence of the decay curves and the correlation areas. This was beyond the scope of this study.

5.4 Discussion of Other Correlation Characteristics

The discussions in paragraphs 5.1 through 5.3 have been oriented toward defining the behavior of a narrow band cross-correlation in terms of the three major variables of separation distance, time displacement, and frequency. Although the general behavior is determined by these variables, there are other characteristics which must be described for a complete understanding of the narrow band cross-correlation data. Some of these topics are: dispersion, behavior with relative location within the flow, separability of the spatial variables, and a non-constant convection velocity.

If the flow were strongly dispersive it would no longer be possible to separate the cross-correlation into a simple decay curve and phase curve. The flow would then have two characteristic velocities, one associated with the envelope of the cross-correlation, and one associated with the phase. These can be characterized as a group velocity and a phase velocity. For a non-dispersive flow, these two velocities are the same and the cross-correlation is easily separated. Other experimenters have shown slight dispersive behavior in experiments involving subsonic Mach numbers. In this experiment, the Mach number was relatively high, usually near 3.5. At this Mach number, small variations in frequency were buried in the high convection velocity--if they existed at all.

If a flow is dispersive, broad band cross-correlations will have a broad peak rather than a sharp one. The broadband cross-correlations from this experiment are as sharply peaked as the autocorrelations suggesting significant differences in convection velocity do not exist. Another measure of dispersion is nonlinearity of the phase angle (non-constant K as defined in par. 5.1). Most of the phase plots were approximately linear to within the statistical scatter. Any significant deviations from linearity occurred at reattachment or separation or near step faces for specific frequency ranges. The behavior in these regions can be associated with complex behavior inside the region of separated flow (some of these phenomena are discussed in sec. 4) where reverse flow, or lateral convection velocities may introduce an anomaly similar to dispersion. Since the flow was only dispersive over small regions of the flow, and small ranges of frequencies, the flow was considered

to be generally nondispersive. Complex phenomena associated with the inside of the separation flow region are subjects for further detailed study.

The variation of the location of maximum resonance coherence in the frequency domain with distance from the step face indicates that the cross-correlation is a function of position in the flow as well as of separation distance. This effect would be particularly pronounced for frequencies near the resonance. Even though this effect can be significant, in general, the dependence on separation distance dominates. The decay curves presented in section 4 have had all data for any one region of flow, irrespective of location, lumped together. The fact that there is a dependence on physical distance would be expected to have introduced some of the scatter present in those data. Further research (acquisition of statistical quantities of data) will be necessary to separate the dependence on physical distance from the dependence on separation distance or to establish the validity of ignoring the former as was done here.

For ease of description, the cross-correlation is normally assumed separable in the two spatial coordinates. An attempt was made to check this assumption. Although there were not a statistically significant number of points, the data indicated that the assumption of separability was valid to within the scatter of the data. However, there generally seemed to be a tendency for the rate of lateral decay to decrease with increased separation distance in the longitudinal direction (see sec. 4). Further research will be required to accurately determine to what extent separability exists in the spatial coordinates. Reference 1 presented a discussion on the expected error introduced in the equal correlation contours, and until sufficient statistical confidence can be placed in a conclusion, users of the separated mathematical functions should be aware that a considerable error may possible be thereby introduced.

As discussed in paragraphs 4.1 and 4.3, the convection velocity does not appear to be constant. The general behavior indicates a rapidly varying convection velocity for small separation distances, becoming asymptotic to another velocity for larger separation distances. This suggests that the source of the coherent portion of the pressure signature moves rapidly from one stratum of the boundary layer to another.

For forward-facing steps and undisturbed flow, the initial velocity is low, suggesting the signature originates in a low-velocity stratum. The velocity rapidly becomes asymptotic to what appears to be nearly the free stream velocity. An eruption type of process, such as already suggested by numerous flow mechanism and theoretical studies would result in just such behavior. There was not sufficient definition in the shock-disturbed flow to demonstrate a non-constant convection velocity.

However, for aft-facing steps before reattachment, higher convection velocities were calculated for small separation distance than for larger separation distances where the latter actually traversed the region of reattachment. Behind an aft-facing step, the boundary layer velocity varies markedly for different regions of flow. It is probable that the drop in velocity with separation distance is a reflection of this phenomenon, since the convection velocity has been normalized to the constant free-stream velocity. If an accurate description of the boundary layer velocity were available, the

convection velocity would be expected to demonstrate an increasing velocity with separation distance when normalized by the boundary layer velocity. After reattachment, where the boundary layer velocity is approximately constant, the aft-facing steps indicate the usual behavior of increasing velocity with separation distance.

The fact that the convection velocity is not constant does not effect the arguments about the coordinate transformations presented in paragraphs 5.1 and 5.2 because the curve $\xi_x = U_c\tau$ is still single valued. The only difference is that the parallelograms described in paragraph 5.2 will be slightly warped.

5.5 Mathematical Description of the Cross-Correlation

If the cross-correlation is assumed to be separable in the retarded time coordinate system (see par. 5.1) and also separable in the two spatial coordinates, it is also assumed that the decay in the lateral and longitudinal direction are exponential

$$\left\{ \frac{P_{\alpha\beta}(\xi_x, \xi_z)}{\sqrt{P_\alpha P_\beta}} = \sqrt{\gamma^2_{\alpha\beta}(\xi_x, \xi_z)} = e^{-\alpha\frac{|\xi_x|}{\theta}} e^{-\beta\frac{|\xi_z|}{\theta}} \right\} \tag{39}$$

the normalized narrow band cross-correlation in the fixed frame of reference can be written as:

$$R(\xi_x, \xi_z, \tau) = e^{-\alpha\frac{|\xi_x|}{\theta}} e^{-\beta\frac{|\xi_z|}{\theta}} \frac{\sin\frac{\omega_o}{2Q}(\tau - \tau_o)}{\frac{\omega_o}{2Q}(\tau - \tau_o)} \cos\omega_o(\tau - \tau_o) \tag{40}$$

where $\tau_o = \xi_x / U_c(\xi_x)$ can be determined from the convection velocity curves presented in sec. 4, and Q, the dynamic amplification factor for structure is related to the bandwidth of the contributing frequencies of the forcing function by: $\Delta = \omega_o/Q$.

Table 4 summarizes the decay rates α and β as determined in section 4. Again, it is important to note that the decay rates for frequencies other than those presented cannot be easily interpolated from the given data for reasons discussed in paragraph 5.3.

5.6 Comparison of Experiment and Theory

A few theoreticians have attempted to analytically describe the flow phenomena producing fluctuating pressures at a wall beneath a turbulent boundary layer. By so doing, they have described certain general dependencies and/or characteristics of the FPL's. This section is intended to briefly summarize

TABLE 4

SUMMARY OF COEFFICIENTS

Flow	Normalized Frequency, $\omega\theta/U_\infty$	α	β
Undisturbed M 3.45	0.01	0.060	0.050
	0.04	0.035	0.055
	0.16	0.025	0.160
Aft-facing step M 1.41	0.01	0.025	0.014
	0.04	0.050	0.030
	0.16	0.045	0.035
Aft-facing step M 3.48	0.01	0.060	0.011
	0.04	0.060	0.080
	0.16	0.100	0.100
Forward-facing step M 3.45	0.01	0.050	0.075
	0.04	0.035	0.090
	0.16	0.040	0.020
Shock-disturbed flow M 3.45	0.01	0.100	0.100
	0.04	0.100	0.350
	0.16	0.125	0.195

the degree of agreement or disagreement between these theories and the experimental results of this study.

Kovasznay (ref. 10), proposed an analytical model describing three major sources for the fluctuating pressures in supersonic turbulent boundary layers. He was able to show that the sound mode made a negligible contribution as compared to other sources (given by him as entropy and vorticity modes). He indicated the energy spectrum at 0.5δ from the wall was comparable in frequency distribution of energy to the spectrum measured at the wall.

In 1953, he indicated the major source to be approximately one-quarter of the way out from the wall. However, the convection velocities for small separations correspond to portions of the velocity profile much closer to the wall. If it is assumed that the convection velocity of the pressure signature reflects the velocity of the boundary layer stratum in which it is to be found, the data suggest a source nearer the wall. Kovasznay also assumed a frozen pattern structure for the pressure signature source (an assumption which is often employed by theoreticians). If the sources move rapidly from the vicinity of the wall to the outer strata of the boundary layer, a flow model which could explain the variation of convection velocity with separation distance, and if a decay mechanism exists which dissipates old sources at the same rate as new ones are produced, a correlation with a decay primarily dependent on separation distance (the addition of new sources) would be suggested. The data examined in this study did indicate such a separation distance dependent decay.

Willmarth (ref. 11) concluded from his model that there was not any dependence on Mach number or Reynolds number of the root mean square pressure, but only a direct proportionality to dynamic pressure. A Mach number dependence was shown to exist in ref. 1. He also assumed a constant convection velocity. However, the data indicated that for small separations, the convection velocity varies with separation. Willmarth concluded that the lateral correlation coefficient ($\xi_x = \tau = 0$) was reduced to a value of about 0.5 at a distance $\xi_z = \delta^*$ for subsonic flow. The data for M 3.45 undisturbed flow suggest a faster decay for all bands of frequencies examined. The data indicate a rather narrow strip in which the pressures are well correlated.

In 1960, Tack et al. (ref. 12) described a model which developed a narrow band cross-correlation mathematical description similar to that developed from this study, however, he transformed to a frame moving with the boundary layer while the present data suggests a retarded time transformation. The discussion in section 5 indicates why a Galilean transformation is not capable of matching the data, whereas a time retarded transformation is. Similarly, Bull (ref. 13) used the Galilean transformation and found a dependence of the correlation amplitude ξ_x/U_c rather than on ξ_x as is demonstrated by the data. Both Tack and Bull showed only fair agreement with data possibly for this reason. In addition, the assumption of constant convection velocity or the choice of an average convection velocity (based on the separation distance divided by the time displacement required for the cross-correlation maximum to reach the second transducer) could spread the data sufficiently as to somewhat mask the characteristics described in this study: (1) a time retarded transformation required to achieve separability of the variables, and (2) a nonconstant convection velocity exists for small separations. Insufficient data actually exists at very close spatial separations to indicate whether the pressure source is continually changing its convection velocity within a separation distance of $\xi_x/\theta \leq 10$, or whether the convection velocity is somewhat constant immediately after formation of the source until a sudden "popping" of the source causes it to jump into another, higher velocity stratum.

Tack et al. drew some other conclusions from their analytical model. They successfully predicted the observable faster rolloff of the power spectrum above a characteristic cutoff frequency for supersonic undisturbed flow. They additionally predicted a faster decay for the higher frequencies. In actuality, as shown in previous discussions, the decay of the narrow band

cross-correlation has unusual frequency dependencies in disturbed flow, and a symmetric frequency dependence for undisturbed flow (mid-frequency peak with faster decays at low and high frequencies). Tack also concluded that the broad band cross-correlation was weighted in preference to those frequencies which retain coherence the longest, but as stated above, the frequency range with highest coherency varies with the kind of flow, the spatial separation, and possibly with the Mach numbers.

Gardner (ref. 14), posed a model for the boundary layer FPL's on the basis of the Navier-Stokes equations which, because of his development, restricted the analysis to frequencies $\omega\delta^*/U_\infty \gg 1$. Since this is in the frequency range above the data for this study, or where the psd is dropping at a rapid rate - predicted by Gardner to be 9 dB/octave and indicated by the data to be - on the average - 10 dB/octave - no real comparisons can be made. In the region of frequencies covered by this theory, the levels are very low, and the frequencies are too high to excite significant structural response.

Lilley, in an early note, predicted that the ratio of rms pressure to dynamic pressure was proportional to the coefficient of friction (essentially Mach number-independent unless compressibility becomes important). The data indicate a Mach number dependence for those Mach numbers investigated ($M_\infty \leq 5.0$). In reference 15, Lilley posed a theoretical model which attributed the production of the FPL's to vorticity and sound modes. As a result, the theory predicts an increase in the ratio of rms pressure to wall shear stress with Mach number. Kistler and Chen data (ref. 16) are used to verify the trend. In contrast, data from this study (ref. 1) and data from in-flight measurements (ref. 17) indicate a decrease with Mach number of the ratio of rms pressure to dynamic pressure. The data from Kistler and Chen are for small spatial separations where the low average convection velocities were measured. In addition, pressure levels and spectral shapes quoted from their data resemble thickened boundary layer data.

In reference 15, Lilley predicted a low-frequency rolloff of the PSD as shown on glider data by Hodgson. Some unpublished data from a supersonic airplane would suggest that the upward trend of the PSD level in the low frequencies (as frequencies are reduced) always seen from wind tunnel measurements is indeed correct. Thus, the glider data still stand uniquely alone in such a low frequency rolloff. Perhaps part of the difficulty in comparing data with Lilley's theory is his neglect of the turbulence - turbulence terms, though in reference 18, Lowson successfully describes some aspects of the flow by also neglecting turbulence - turbulence terms in favor of mean shear-turbulence terms (for the attached boundary layer). Lowson discards viscosity and predicts the rms pressure divided by dynamic pressure to have nearly the dependence indicated by the data and the pressure divided by wall shear stress to be a constant. However, he states that any perturbations or external noise will negate these proportionalities. Lowson predicts that the major contribution to the FPL's is generated in a stratum where $U_c/U_\infty = 0.5$. This agrees with the results of this study. Lowson goes on to discuss the possibility of an eruption-like process to account for the variation in convection velocity. The data from this study are consistent with such a phenomological description for the major source since no dispersion effects were observed, and within the data scatter, it appeared that all frequencies examined moved with the same velocity.

Lowson discusses possible characteristics of separated flow, and on the basis of his model, suggested that most of the source in separated flow is found in a region of high shear with very low velocity (≈ 0). The data of this study from separated flow would indicate otherwise, since the convection velocities in these regions were similar fractions of the detached boundary layer velocity, as for an attached flow.

Houbolt, with his engineering model (ref. 19), was not too successful in predicting either the rms pressure to dynamic pressure ratio versus Mach number or in predicting the shape of the PSD according to the data summarized and quoted in reference 8. He does, however, show a more logical dependence of the wall pressure on the free-stream pressure and the Mach number than could be assumed with the dependence on dynamic pressure. It seems untenable to predict magnitudes of pressure fluctuations considerably larger than the atmospheric pressure nearby which are obviously going to be influenced by nonlinearities before these magnitudes are achieved.

Black (ref. 20) proposes a theoretical model which has considerable success in comparing with the data. For example, the model predicts a stretching of the original eddy (or vortex) as it moves downstream. One characteristic of the data could be explained by such a mechanism (see par. 4.1). The model predicts an eruption process which is consistent with the convection velocity data. This model, similar to Lilley's, predicts a dependence on wall shear stress for the fluctuating pressure (undefined as yet). The model also predicts increased levels due to positive pressure gradients and decreased levels when negative pressure gradients are present. Such dependencies are indicated in general by the data (ref. 8, fig. 10). Black's model indicates a dependence of the vortex generating shear stress location within the boundary layer on Reynolds number. This results in a different spectral dependence than previously considered.

Black's model entails many more details such as spectral spikes, different velocities for low and high frequencies which are smeared due to a "sharing" phenomenon that makes their subtle differences appear as scatter on the mean velocity, etc. Considerable work will be involved in validating or disproving the proposed model, but of those presented, it does seem to agree most favorably with the data.

6. CONCLUSIONS

The data, as examined in this study, have indicated certain basic conclusions which have been substantiated by mathematical concepts where possible. These conclusions, including some interesting and unique concepts concerning the fluctuating pressures at a wall beneath a turbulent boundary layer, are:

(1) The convection velocity of a particular pressure signature beneath either an undisturbed turbulent boundary layer, or one disturbed by forward-facing or aft-facing steps, exhibits a rapid change within small separation distances followed by a long region in which the convection velocity remains constant. As a result of this, any graph of correlation versus a structural-type parameter of the $\xi_x\omega/U_c$ variety will indicate a variation at low values. This variation may well be attributable to convection velocity variations rather than dispersion effects. The shock-disturbed flow did not exhibit a region of rapid change. No major dispersive effects were observed for the frequency ranges examined.

(2) The narrow band data substantiates the mathematical model which permits separation of the time and space domains for a retarded time frame of reference. The commonly used Galilean transformation, being approximately correct for very wide band analysis, is not valid for narrow band analysis. This indicates a spatial dependence of the correlation with the temporal dependence determined by bandwidth and center frequency.

(3) Because of unusual frequency dependencies of the spatial decay within regions of disturbed flow, statistically significant quantities of data must be acquired to define the dependence on location within the disturbed flow, Mach number, and geometry.

(4) An unusual source of FPL's was hypothesized for an aft-facing step that produced the measured energy in the low frequencies and the lateral convection velocity component. Insufficient data exists to exactly define its dependence on geometry, or its existence in other aft-facing step configurations (such as axially symmetric three-dimensional bodies), but it is presumed to be the source which produced the FPL's measured directly behind the step face in this experimental study.

(5) The mathematical expression in the fixed frame of reference for the one-dimensional cross-correlation of narrow band data may be written in the form

$$R_x(\xi_x, \tau) = \frac{P_{a\beta}(\xi_x)}{\sqrt{P_a P_\beta}} \frac{\sin \frac{\Delta}{2}\left[\tau - \frac{\xi_x}{U_c(\xi_x)}\right]}{\frac{\Delta}{2}\left[\tau - \frac{\xi_x}{U_c(\xi_x)}\right]} \cos \omega_o \left[\tau - \frac{\xi_x}{U_c(\xi_x)}\right] \qquad (41)$$

Douglas Aircraft Company
Santa Monica, California
November 15, 1967

7. REFERENCES

1. Speaker, W. V.; and Ailman, C. M.: Spectra and Space-Time Correlations of the Fluctuating Pressures at a Wall Beneath a Supersonic Turbulent Boundary Layer Perturbed by Steps and Shock Waves. NASA CR 486, May 1, 1965.

2. Douglas Aircraft Company: Trisonic One-Foot Wind Tunnel; Description of the Facility and Provisions for Testing. Report No. ES 29278, January 1969.

3. Murphy, J. S.; et. al.: Wind Tunnel Investigation of Turbulent Boundary Layer Noise as Related to Design Criteria for High Performance Vehicles. NASA TN D-2247, April 1964.

4. Bendat, J. S.: Principles and Application of Random Noise Theory. John Wiley and Sons, New York, 1958.

5. Blackman, R. B.; and Tukey, T. W.: The Measurement of Power Spectra. Dover Publications, New York, 1958.

6. Plumbee, H. E.; et. al.: A Theoretical and Experimental Investigation of the Acoustical Response of Cavities in an Aerodynamic Flow. WADD TR-61-75, March 1962.

7. Bendat, J. S.; and Piersol, A. G.: Measurement and Analysis of Random Data. John Wiley and Sons, New York, 1966.

8. Ailman, C. M.: On Predicting Fluctuating Pressure at a Wall Beneath a Turbulent Boundary Layer. Douglas Aircraft Company Paper No. 4331, April 1967.

9. White, P. H. (Staff of Measurement Analysis Corp.) Communicated in private conversation.

10. Kovaszany, L. S. G.: Turbulence in Supersonic Flow. J. of the Aeron. Sci., vol. 20, no. 10, October 1953.

11. Willmarth, W. W.: Statistical Properties of the Pressure Field in a Turbulent Boundary Layer. WADC TR-59-676, March 1961.

12. Tack, D. H.; et. al.: Wall Pressure Correlations in Turbulent Airflow. J. Acoust. Soc. Am., vol. 33, no. 4, April 1961, pp. 410-418.

13. Bull, M. K.: Space Time Correlations of the Boundary Layer Pressure Field in Narrow Frequency Bands. ASD-TDR-62-722, November 1963.

14. Gardner, S.: On Surface Pressure Fluctuations Produced by Boundary Layer Turbulence. Acustica, vol. 16, no. 2, 1965/66, pp. 67-74.

15. Lilley, G. M.: Wall Pressure Fluctuations Under Turbulent Boundary Layers at Subsonic and Supersonic Speeds. Cranfield Coll. of Aeronautics, COA Note 140, March 1963.

16. Kistler, A. L.; and Chen, W. S.: The Fluctuating Pressure Field in a Supersonic Turbulent Boundary Layer. JPL Tech. Rep. No. 32-277, August 1962.

17. Belcher, P. M.: Predictions of Boundary-Layer Turbulence Spectra and Correlations for Supersonic Flight. Presented at the 5th Int'l. Acoustical Congress, Liege, Belgium, September 1965.

18. Lowson, M. V.: Pressure Fluctuations in Turbulent Boundary Layers. NASA TN D-3156, December 1965.

19. Houbolt, J. C.: On the Estimation of Pressure Fluctuations in Boundary Layers and Wakes. ARAP Rep. no. 90, June 1966.

20. Black, T. J.: A New Approach to Wall Turbulence, The Shear Stress Mechanism. Mech. Tech. Inc., July 1967 (to be published).